

🍅 HUMAN TOMATO: TEXT-ALIGNED WHOLE-BODY MOTION GENERATION

Shunlin Lu^{*†♣◇}, Ling-Hao Chen^{*†♣◇},

Ailing Zeng^{‡◇}, Jing Lin^{†♣◇}, Ruimao Zhang^{§♣}, Lei Zhang[◇], Heung-Yeung Shum^{§♣◇}

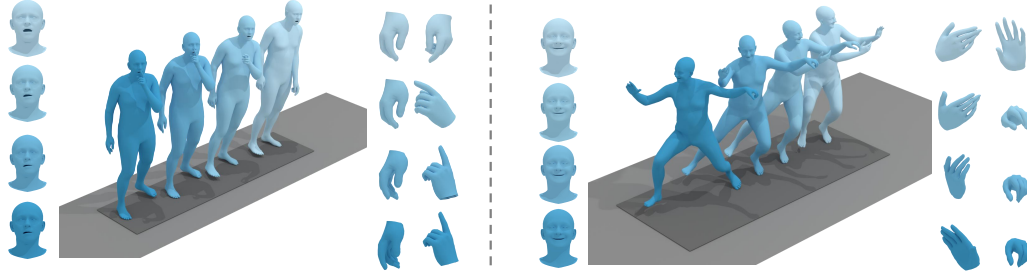
♣ Tsinghua University

◇ International Digital Economy Academy (IDEA)

♠ School of Data Science, The Chinese University of Hong Kong, Shenzhen (CUHK-SZ)

{shunlinlu0803, thu.lhchen}@gmail.com

<https://lhchen.top/HumanTOMATO>



(a) stand and shush, angrily.

(b) Yang-style 40 form Tai Chi Competition routine step 34, happily.

Figure 1: The proposed HumanTOMATO can generate text-aligned whole-body motions with vivid and harmonious face, hand, and body motion. We show two generated qualitative results.

ABSTRACT

This work targets a novel text-driven **whole-body** motion generation task, which takes a given textual description as input and aims at generating high-quality, diverse, and coherent facial expressions, hand gestures, and body motions simultaneously. Previous works on text-driven motion generation tasks mainly have two limitations: they ignore the key role of fine-grained hand and face controlling in vivid whole-body motion generation, and lack a good alignment between text and motion. To address such limitations, we propose a Text-aligned whOle-body Motion generATIOn framework, named HumanTOMATO, which is the first attempt to our knowledge towards applicable holistic motion generation in this research area. To tackle this challenging task, our solution includes two key designs: (1) a Holistic Hierarchical VQ-VAE (*aka* H²VQ) and a Hierarchical-GPT for fine-grained body and hand motion reconstruction and generation with two structured codebooks; and (2) a pre-trained text-motion-alignment model to help generated motion align with the input textual description explicitly. Comprehensive experiments verify that our model has significant advantages in both the quality of generated motions and their alignment with text.

1 INTRODUCTION

Recent years have seen an explosion of huge demand for generating high-quality 3D human motions in many scenarios, such as games, films, animation, and robotics. To reduce laborious efforts in animation creation, recent studies (Tevet et al., 2023; Chen et al., 2023b; Zhang et al., 2022; 2023) attempt to generate human motions with textual description in a natural interactive way and have achieved rapid progress in related research areas.

However, the generated motions from existing works are still unsatisfactory to meet real application needs. The problem is mainly due to two aspects. First, *existing text-driven motion generation models can only generate body-only motions rather than whole-body motions, which are highly expressive yet much more challenging*. On the one hand, the mentioned challenge comes from the

*Co-first author. Listing order is random.

†This work was done when Shunlin Lu, Ling-Hao Chen, and Jing Lin were interns at IDEA.

‡Project lead.

§Corresponding authors.

limited availability of whole-body motion data. On the other hand, whole-body motion is much more complex, where fine-grained motions of body, hand, and face should be well generated. How to model whole-body human motions is still under-explored. Second, *the generated motions lack semantic alignment with the textual description*. Existing methods adopt CLIP (Radford et al., 2021) or Large Language Models (LLMs) (Raffel et al., 2020) to provide language guidance for motion generation (Zhang et al., 2022; Tevet et al., 2023; 2022; Jiang et al., 2023). However, their alignment supervision is provided at frame level and lacks sufficient understanding of a motion at its whole sequence level. As a result, they often fail to distinguish some scenarios, such as “walking in a clockwise circle” and “walking in a counter-clockwise circle”, which requires understanding motions at sequence level rather than frame level. Such a drawback severely limits the ability to generate motions well-aligned with textual descriptions.

To tackle the above issues, we propose a novel Text-aligned whOle-body Motion generATIOn framework (HumanTOMATO). The framework includes two key designs. First, *a holistic hierarchical discrete modeling strategy for body and hand motions is proposed for reconstructing and generating whole-body motions vividly*. As whole-body motion is a kind of high-dimensional spatio-temporal signal, in the first stage, we propose a Holistic Hierarchical VQ-VAE (*aka* H^2VQ) to compress the motion into two-level discrete codes for body and hand, respectively. In contrast, a naïve solution that simply replaces body-only motions with whole-body motions or directly increases the size of the codebook is almost in vain. The key insight of our H^2VQ is learning informative and compact representations of fine-grained whole-body motions at very low bit rates. Based on the two-level discrete codes, in the second stage, we propose a Hierarchical-GPT to predict the hierarchical discrete codes of body and hand in an auto-regressive fashion. For the remaining facial motions, we generate facial expressions with a Facial conditional VAE (cVAE). Second, *a pre-trained text-motion-alignment model is introduced to enhance the textual alignment of generated motions for the first time*. For pairwise text-motion data, we pre-train a motion encoder and a text encoder, namely TMR (Petrovich et al., 2023), in a contrastive learning manner (Radford et al., 2021). Different from previous work (Zhang et al., 2022; Tevet et al., 2023; 2022; Jiang et al., 2023), we use text embedding of TMR as a language prior other than the embedding from CLIP or LLMs. In this way, the TMR provides a motion-aware language embedding for the Hierarchical-GPT to generate discrete motion codes more precisely. It is worth noting that, during training, merely supervising the prediction of discrete code tokens of body and hand is insufficient as it lacks supervision on the semantics of global motion sequence and will cause error accumulation in auto-regressive prediction. Therefore, with the text-motion similarity measured by TMR, we additionally provide text-motion alignment supervision to supervise the alignment of generated motion sequences and texts explicitly.

With these key designs, compared with previous text-driven motion generation works, HumanTOMATO can generate whole-body motions that are semantically aligned with textual descriptions, as illustrated in Figure 1. To evaluate the alignment between generated motions and input texts, we further revisit the previous retriever used for evaluating text-motion alignment and find that its retrieval ability is worse than TMR. Hence, we introduce two new criteria ($TMR-R-Precision^{(256)}$ and $TMR-Matching-score$), which are more accurate and challenging to evaluate the text-motion alignment in motion generation.

Before delving into details, we carefully clarify our main contributions as follows:

- To the best of our knowledge, we propose the challenging Text-driven whOle-body Motion generATIOn task for the first time and design a model (**HumanTOMATO**) to generate vivid whole-body motions that are well aligned with texts.
- To tackle the challenging whole-body motion generation problem, we introduce a H^2VQ for fine-grained body and hand motion reconstruction. Accordingly, we develop a Hierarchical-GPT combined with facial cVAE to generate whole-body motions.
- To enhance the consistency and alignment between texts and motions, we pre-train text-motion-aligned encoders via a contrastive objective and introduce a sequence-level semantic supervision to help motion-text alignment.
- We propose two new criteria ($TMR-R-Precision^{(256)}$ and $TMR-Matching-score$), which are more accurate and challenging for evaluating text-motion alignment.

We evaluate HumanTOMATO on both whole-body (Lin et al., 2023a) and body-only (Guo et al., 2022) motion generation benchmarks and answer four research questions based on our contributions. Experiments affirm the vividness and alignment of our generated motions with text inputs.

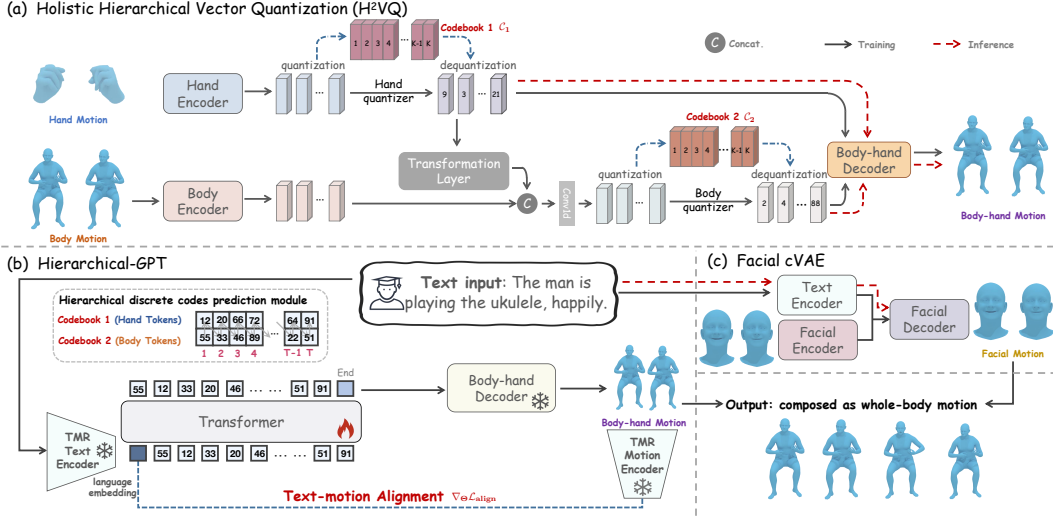


Figure 2: The framework overview of the proposed text-driven whole-body motion generation. (a) Holistic Hierarchical Vector Quantization (H²VQ) to compress fine-grained body-hand motion into two discrete codebooks with hierarchical structure relations. (b) Hierarchical-GPT using motion-aware textual embedding as the input to hierarchically generate body-hand motions. (c) Facial text-conditional VAE (cVAE) to generate the corresponding facial motions. The outputs of body, hand, and face motions comprise a vivid and text-aligned whole-body motion.

2 METHODOLOGY

2.1 PROBLEM FORMULATION

We clarify notations and set up the novel research problem of text-driven **whole-body** motion generation. Given a text description \mathbf{t} of a human motion, such as “*The man is playing the ukulele happily.*”, the model should generate a vivid whole-body motion $\mathbf{m} = [\mathbf{m}_1, \mathbf{m}_2, \dots, \mathbf{m}_L] \in \mathbb{R}^{L \times d}$ aligned with the text description, where L and d denote the number of frames and the dimension of the motion in each frame, respectively. As whole-body motion comes up with hand, body, and face motions, we can also decompose the \mathbf{m} as $\{\mathbf{m}^H, \mathbf{m}^B, \mathbf{m}^F\}$ respectively, where $\mathbf{m}^H \in \mathbb{R}^{L \times d_h}$, $\mathbf{m}^B \in \mathbb{R}^{L \times d_b}$, $\mathbf{m}^F \in \mathbb{R}^{L \times d_f}$, $d = d_h + d_b + d_f$. Mathematically, we formulate the text-driven whole-body motion generation as follows:

$$\Theta^* = \arg \max_{\Theta} P_{\Theta}(\mathbf{m} | \mathbf{t}),$$

where Θ denotes the model parameters and $P_{\Theta}(\cdot)$ denotes the motion distribution, respectively.

The content for the subsequent sections is outlined as follows. In Section 2.2, we first introduce H²VQ to learn fine-grained discrete motion codes for both body and hands. Then we present the Hierarchical-GPT Module in Section 2.3, which is designed to predict the text-aligned discrete motion codes for whole-body motions. Since the facial expressions are usually deterministic to textual descriptions, we adopt the method described in Petrovich et al. (2022) to train a facial conditional VAE, thereby generating detailed expressions directly. For whole-body motion generation, we integrate motions from the body, hands, and face to produce the final output. Notably, when introducing our Hierarchical-GPT, we also explore how a text-to-whole-body motion retrieval model can benefit the text-motion alignment explicitly in Section 2.4.

2.2 LEARNING DISCRETE WHOLE-BODY REPRESENTATIONS

Vanilla Motion VQ-VAE. Motion VQ-VAE aims to learn discrete representations of human motions in an encoding-decoding fashion. Specifically, VQ-VAE recovers motions by using an auto-encoder and learns a codebook $\mathcal{C} = \{\mathbf{e}_k\}_{k=1}^K$, where K denotes the codebook size and \mathbf{e}_k indicate the k -th embedded representation in the codebook. Given a vector \mathbf{z} and the quantizer $\mathcal{Q}(\cdot; \mathcal{C})$, the quantized vector should be the element selected from the codebook \mathcal{C} that can minimize the reconstruction error of \mathbf{z} as,

$$\hat{\mathbf{z}} = \mathcal{Q}(\mathbf{z}; \mathcal{C}) = \arg \min_{\mathbf{e}_k} \|\mathbf{z} - \mathbf{e}_k\|_2^2.$$

In a vanilla VQ-VAE, $\mathbf{z} = \text{Enc}(\mathbf{m})$ indicates the latent code extracted from a motion encoder $\text{Enc}(\cdot)$. Thus VQ-VAE can be optimized by,

$$\mathcal{L} = \|\mathbf{m} - \text{Dec}(\mathcal{Q}(\mathbf{z}; \mathcal{C}))\|_2^2 + \alpha \|\mathbf{z} - \text{sg}(\hat{\mathbf{z}})\|_2^2, \quad (1)$$

where α is the hyper-parameter, $\text{sg}(\cdot)$ is the stop-gradient operation and $\text{Dec}(\cdot)$ indicate the motion decoder. Different from traditional methods, the codebook \mathcal{C} in motion VQ-VAE is optimized by exponential moving average (EMA) and codebook reset (Code Reset) operations following [Razavi et al. \(2019\)](#); [Van Den Oord et al. \(2017\)](#); [Zhang et al. \(2023\)](#). Although the motivation behind discrete vector quantization in vanilla VQ-VAE is capable of compressing human motions, the quantization error present in motions can also compromise the quality of motion reconstruction, particularly for whole-body motion generation with massive details. In practice, an intuitive solution to address this would be to increase the size of the codebook. However, adopting such a scheme would evidently lead to an increase in the computational cost and quickly encounter performance bottlenecks (see results in Section 3.4).

Holistic Hierarchical VQ-VAE. Recently, the Residual Vector Quantization technique, also known as RVQ ([Barnes et al., 1996](#); [Zeghidour et al., 2021](#); [Yao et al., 2023](#)), has significantly advanced the development of music generation task ([Défossez et al., 2022](#); [Copet et al., 2023](#)). Technically, RVQ iteratively quantizes the quantization error at each level from the previous one, reducing quantization errors effectively while maintaining a low memory cost of the codebook (see Appendix C.2 for details). Motivated by this ([Défossez et al., 2022](#)), we propose a novel Holistic Hierarchical Vector Quantization scheme, shorted by H²VQ, into the field of motion generation. Unlike RVQ, we incorporate the kinematic structure prior to the H²VQ modeling, enabling it to learn compact representations of fine-grained whole-body motions at an extremely low bit rate. Given the distinct differences in amplitude and frequency between body and hand motions, we have further designed two separate encoders and codebooks to learn discrete representations for body and hand motions.

The architecture of our proposed H²VQ is illustrated in Figure 2(a). In the encoding phase, we input hand and body motions, obtaining hand and body tokens through the hand encoder $\text{Enc}^H(\cdot)$ and body encoder $\text{Enc}^B(\cdot)$, respectively. The learned hand tokens are further quantized by the Hand Quantizer $\mathcal{Q}^H(\cdot; \mathcal{C}^H)$ as \mathbf{z}^H . Since the body motions are usually highly associated with some hand gestures ([Ao et al., 2022](#)), to train a more natural and coordinated body codebook, we fuse the body and hand tokens using the $\text{Concat}(\cdot)$ and $\text{Conv1d}(\cdot)$ operations. As shown in Figure 2, before this fusion operation, the quantized hand tokens undergo a transformation through a projection layer. After that, fused tokens are further quantized by Body Quantizer $\mathcal{Q}^B(\cdot; \mathcal{C}^B)$ as \mathbf{z}^B . Finally, the hand tokens \mathbf{z}^H and body tokens \mathbf{z}^B are concatenated together and fed into the Body-hand Decoder to reconstruct the body-hand motions precisely.

During the training phase, the primary goal is to reconstruct motions while concurrently updating the two codebooks through the EMA and Code Reset operations ([Razavi et al., 2019](#); [Van Den Oord et al., 2017](#); [Zhang et al., 2023](#)). In the inference phase, after obtaining quantized code indices, the Body-hand Decoder can generate body-hand motions by querying the respective codebooks with obtained code indices. The detailed algorithmic flows for both training and inference phases can be found in Appendix C.

2.3 HIERARCHICAL WHOLE-BODY MOTION GENERATION

Given the two precise quantized codebooks of H²VQ, the motion sequence should be generated by using the corresponding decoders and quantized codes. The previous popular approach is to predict code indices in GPT-like auto-regressive fashion ([Zhang et al., 2023](#)). Since the proposed H²VQ requires the usage of two codebooks with structure relations, the aforementioned approach is not applicable. To better model the natural coherence of body-hand motions, we design a hierarchical discrete codes prediction module, named Hierarchical-GPT, which is illustrated in Figure 2(b), for generating body-hand motions.

Hierarchical-GPT. The Hierarchical-GPT is built upon a transformer-based architecture, where the first input token is a textual embedding. With the input body-hand motion $\mathbf{m}^B = [\mathbf{m}_1^B, \mathbf{m}_2^B, \dots, \mathbf{m}_L^B]$ and $\mathbf{m}^H = [\mathbf{m}_1^H, \mathbf{m}_2^H, \dots, \mathbf{m}_L^H]$, we have corresponding code indices, denoted as $\mathbf{I}^B = [\mathbf{I}_1^B, \mathbf{I}_2^B, \dots, \mathbf{I}_{L/r}^B, \text{End}]$ and $\mathbf{I}^H = [\mathbf{I}_1^H, \mathbf{I}_2^H, \dots, \mathbf{I}_{L/r}^H, \text{End}]$, where ‘End’ indicates the end token and r denotes the down-sampling rate, which is used to convert the input motion sequence

to discrete motion tokens. Therefore, as shown in Figure 2(b), the code indices prediction can be formulated as an auto-regressive prediction problem:

$$\begin{aligned}
 P(\mathbf{I}_{1,2,\dots,L/r}^{B,H} | \mathbf{t}) &= \prod_{s=1}^{L/r} P(\mathbf{I}_s^{B,H} | \mathbf{I}_{<s}^{B,H}, \mathbf{t}) \\
 &= \prod_{s=1}^{L/r} P(\mathbf{I}_s^B | \mathbf{I}_{<s}^{B,H}, \mathbf{t}) \cdot P(\mathbf{I}_s^H | \mathbf{I}_s^B, \mathbf{I}_{<s}^{B,H}, \mathbf{t}),
 \end{aligned}
 \tag{2}$$

where we first predict the body token index and then predict the hand token index at each down-sampled timestamp s . As shown in Figure 2(b), the first token is the textual embedding of the input text. Here we leverage a pre-trained text encoder to extract such an embedding. Please refer to Section 2.4 for more details. In practice, we train the prediction transformer with casual self-attention (Vaswani et al., 2017). As the Hierarchical-GPT aims to predict code indices, our model is optimized with the cross-entropy loss \mathcal{L}_{CE} . The training details are available in Appendix B.3.

Facial conditional VAE. As the facial expression is partially independent of body and hand motions while highly related to the given facial descriptions and even speech, we generate the facial motion with a Facial conditional VAE (cVAE) based on given expression texts. Motivated by TEMOS (Petrovich et al., 2022), our Facial cVAE, shown in Figure 2(c), is composed of a facial encoder, a text encoder, and a facial decoder, which are optimized with the facial reconstruction loss, KL loss, and the cross-modality loss. In the inference stage, given the textual description, the text encoder and motion decoder will generate the diverse face motion according to the expression in the given text and the motion length. The training details are available in Appendix B.4.

2.4 PRE-TRAINED TEXT-MOTION RETRIEVAL MODEL AS A PRIOR

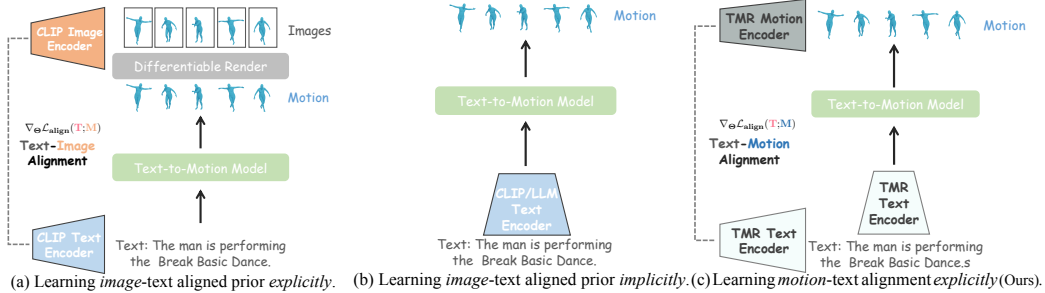


Figure 3: Technical comparisons on introducing language priors of existing methods.

In existing pre-trained models, there often exists a notable semantic gap between the representation of text and its corresponding motion due to the differences in the granularity of content representation between text and motion. For instance, text may involve a simple verb but its corresponding motion would require a sequence of actions. For the text-to-motion generation task, it is crucial to ensure that the textual embedding extracted from the text encoder is motion-aware. Recent work (Petrovich et al., 2023) tries to bridge the gap between text and motion representations, thereby obtaining a text embedding more conducive to driving motion generation.

As shown in Figure 3(a) and Figure 3(b), we can briefly divide them into two categories. The first is *supervision by an image-text aligned prior explicitly*. As there was no strong text-motion-aligned pre-trained model, MotionCLIP (Tevet et al., 2022) renders the generated motions as images and then supervises the alignment between text and rendered images with the CLIP model. However, the image encoder of CLIP is a strong supervision of static image content understanding, which is quite different from dynamic motion. This supervision will cause the generated motion to be *over-smoothing*, even *stillness* (see Appendix E). Therefore, supervising generated motion via a text-image-aligned prior is inappropriate. The second is *learning with image-text aligned prior implicitly*. Existing attempts (Tevet et al., 2023; Zhang et al., 2023; 2022; Yuan et al., 2023) take the CLIP text embedding as the language prior to the text-motion model training. On the one hand, it learns the motion-text alignment implicitly with pairwise data, and there is no supervision to discriminate whether the generated motion is aligned with the text explicitly. On the other hand, the CLIP text embedding is aligned with visual content, lacking the understanding of dynamic motion clues, which cannot provide sufficient spatial-temporal information to generate text-aligned motion.

Therefore, it is essential to introduce a text-motion-aligned pre-training method, ensuring that the trained text encoder can output textual embeddings more conducive to accomplishing text-to-motion generation tasks, instead of adapting from the image-text-aligned model.

Motivated by Petrovich et al. (2023), we pre-train a motion encoder and a text encoder via aligning Text and Motion in a contrastive way (Radford et al., 2021) through a Retrieval target, named TMR. Different from previous work (Zhang et al., 2022; Tevet et al., 2023; 2022; Jiang et al., 2023), the text embedding of TMR plays the role of motion-aware language prior other than the embedding from CLIP or LLMs, which is beneficial for generating text-aligned motions. In this work, the TMR is re-trained by ourselves. We leave the training details in Appendix D.

Based on the pre-trained TMR, we explore enhancing the alignment between the given text and generated motions from two aspects, which are shown in Figure 3(c). The first is *replacing the CLIP text encoder with the TMR text encoder*. Compared with the CLIP text encoder, the pre-trained TMR text encoder provides text embeddings aligned better with dynamic human motions. With the motion-aware language prior, our model can capture motion sequentiality, directions, and dynamics better than text-image-aligned language prior. The second is *introducing the motion-text alignment supervision with TMR*. When training, we feed the generated motion and the given text into the pre-trained TMR motion encoder and text encoder, respectively, to obtain both motion and text embeddings. Then, we calculate a contrastive loss \mathcal{L}_{align} (Radford et al., 2021) for supervising the motion-text alignment. Accordingly, the weighted contrastive loss $\eta\mathcal{L}_{align}$ is added to the optimization objective, where η is the hyper-parameter. The proposed optimization objective provides explicit supervision for text-motion alignment.

2.5 MODEL TRAINING AND INFERENCE

Model Training. In the first stage, similar to the vanilla VQ (Eqn. 1), H^2VQ is optimized by:

$$\mathcal{L} = \|\mathbf{m} - \text{Dec}(\mathcal{Q}^H(\mathbf{z}^H; \mathcal{C}^H), \mathcal{Q}^B(\mathbf{z}^B; \mathcal{C}^B))\|_2^2 + \alpha (\|\mathbf{z}^H - \text{sg}(\hat{\mathbf{z}}^H)\|_2^2 + \|\mathbf{z}^B - \text{sg}(\hat{\mathbf{z}}^B)\|_2^2). \quad (3)$$

Besides, the codebooks are optimized by EMA and Code ReSet techniques. In the second stage, we train the Hierarchical-GPT with both the cross-entropy loss \mathcal{L}_{CE} and the text-motion alignment loss \mathcal{L}_{align} , overall as $\mathcal{L}_{CE} + \eta\mathcal{L}_{align}$.

Model Inference. In the inference phase, we first extract the text embedding from TMR. Then we feed the TMR textual embedding as the initial token into the Hierarchical-GPT, which then predicts discrete body and hand tokens in an auto-regressive fashion. The body and hand tokens are fed into the Body-hand Decoder to generate text-aligned human motion. Ultimately, incorporating the facial motions produced by the Facial cVAE, we output the comprehensive whole-body motions.

3 EXPERIMENTS

In this section, we evaluate the proposed HumanTOMATO model on both whole-body and body-only motion generation benchmarks. Besides, we will also present ablations on each technical design of our method. We structure the experiments to answer the following **four** research questions (RQs).

- **RQ1:** Does our proposed HumanTOMATO model outperform existing generation methods on the whole-body motion generation task?
- **RQ2:** How do hierarchical discrete representations of whole-body motions help improve the quality of motion generation?
- **RQ3:** How does the pre-trained text-motion retrieval model help the alignment between the generated motions and texts?
- **RQ4:** Why are the proposed evaluation metrics on alignment between generated motions and given texts more accurate and challenging?

3.1 DATASETS AND EVALUATION

3.1.1 WHOLE-BODY AND BODY-ONLY DATASETS

Motion-X (Lin et al., 2023a) is currently the largest 3D whole-body motion-text dataset, which consists of 95,642 high-quality human motions along with 95,642 text captions. In Motion-X,

GRAB (Taheri et al., 2020) is a representative subset with vivid grab motions, which is used for our ablation study.

HumanML3D (Guo et al., 2022) is currently the largest 3D body-only motion-text dataset, which consists of 14,616 high-quality human motions along with 44,970 text captions.

We take the Motion-X dataset to evaluate the whole-body motion generation task and the HumanML3D dataset to perform ablations for verifying the generalizability of our proposed solution to the body-only motion generation setting. We follow Lin et al. (2023a); Guo et al. (2022) to split these datasets into training, validation, and test sets with proportions of 80%, 5%, and 15%.

3.1.2 EVALUATION

We quantitatively evaluate the generated motions from three aspects. (1) **The quality of the generated motions.** *Frechet Inception Distance (FID)* is adopted to measure the gap between the distributions of the generated and real motions. (2) **The alignment between texts and generated motions.** *Matching-score* is used to measure the similarity between texts and the generated motions and *R-Precision^(B)* is used to measure the motion-to-text retrieval accuracy in a B -size retrieval pairwise motion-text set. (3) **Generation diversity.** We use *Diversity* to evaluate the average extracted feature Euclidean distances among 300 randomly sampled motion pairs and use *MModality* to measure the generation diversity within the same given text.

To better evaluate the alignment between generated motions and texts, we additionally introduce new metrics to evaluate text-motion alignment from two aspects: (1) **More accurate evaluation.** Previous works used the feature extractor from Guo et al. (2022) to calculate the *R-Precision^(B)* and *Matching-score*. However, its retrieval accuracy is not as accurate as the TMR described in Section 2.4 (comparison in Section 3.6). Therefore, we introduce *TMR-R-Precision^(B)* and *TMR-Matching-score* to evaluate the text-motion alignment, where the feature extractor is replaced by TMR but not the retriever in Guo et al. (2022). (2) **More challenging evaluation metrics.** Retrieval of corresponding texts in a 32-size set is easier than retrieval in a larger size set. Therefore, we add a new retrieval setting as $B = 256$. The comparison between these two settings will be shown in Section 3.6. Besides, we also provide qualitative comparisons of visualization results.

We compare our HumanTOMATO with existing state-of-the-art baselines. (1) **T2M-GPT:** The T2M-GPT (Zhang et al., 2023) method learns discrete representations for motions at first, and then introduces a GPT-like codes prediction mechanism in the second stage with CLIP prior. (2) **MDM:** MDM (Tevet et al., 2023) is a pioneering work that introduces diffusion models into the field of action generation. (3) **MLD:** Motivated by latent diffusion models (Rombach et al., 2022), MLD (Chen et al., 2023b) learns motion latent representations for motion VAE via a diffusion model.

3.2 IMPLEMENTATION DETAILS

Motion representation. For body-hand motion representations, inspired by the motion representation (H3D-Format) in Guo et al. (2022), we expand the body-only representation to holistic body-hand motion representation. Specifically, the i -th pose is defined by a tuple of root angular velocity $\dot{r}^a \in \mathbb{R}$ along the Y-axis, root linear velocities $(\dot{r}^x, \dot{r}^z \in \mathbb{R})$ on XZ-plane, root height $r^y \in \mathbb{R}$, local joints positions $\mathbf{j}^p \in \mathbb{R}^{3N-1}$, and velocities $\mathbf{j}^v \in \mathbb{R}^{3N}$, where N denotes the number of whole body joints, including both body joints and hand joints. For face motion representations, we follow the Flame Format (Kim et al., 2023) and use $\mathbf{f} \in \mathbb{R}^{50}$ to represent the face expression. Thus, we represent the whole-body motion as $m_i = \{\dot{r}^a, \dot{r}^x, \dot{r}^z, \dot{r}^y, \mathbf{j}^p, \mathbf{j}^v, \mathbf{f}\}$. We conduct a set of ablation studies on HumanML3D based on VAE and VQ-VAE to justify the motion format. Please refer to Appendix B.1 for more details.

Training details. All our experiments are trained with the AdamW (Loshchilov & Hutter, 2019) optimizer using a fixed learning rate of 10^{-4} on $4 \times$ NVIDIA Tesla A100-80GB GPUs and are tested on $1 \times$ NVIDIA Tesla A100-80GB GPU. Training batch size is set to 256 for both H²VQ and Hierarchical-GPT stages. Each experiment is trained for 6,000 epochs during H²VQ stages and 2,000 epochs during Hierarchical-GPT stages. Please refer to Appendix B for more details.

	FID↓	TMR-R-Precision ⁽²⁵⁶⁾			R-Precision ⁽³²⁾			TMR-Matching↓	Matching↓	MModality↑	Diversity↑
		Top1↑	Top2↑	Top3↑	Top1↑	Top2↑	Top3↑	Score	Score		
GT	-	0.500	0.708	0.814	0.407	0.578	0.673	0.768	2.888	-	11.087
T2M-GPT	1.366	0.368	0.553	0.655	0.310	0.446	0.527	0.881	4.316	2.356	10.753
MDM	3.800	0.352	0.547	0.6341	0.310	0.430	0.530	0.840	4.050	2.530	11.400
MLD	3.407	0.385	0.571	0.683	0.333	0.477	0.561	0.883	3.901	2.448	10.420
HumanTOMATO	1.174	0.416	0.603	0.703	0.399	0.555	0.638	0.809	3.894	1.732	10.812

Table 1: Main results of motion generation on Motion-X dataset.

3.3 MAIN RESULTS ANALYSIS (RQ1)

We answer RQ1 from both quantitative and qualitative aspects. (1) *Quantitative results.* We quantitatively compare our method with baselines from generation quality, text-motion alignment, and diversity, which are shown in Table 1. The metrics show that our method wins baseline methods on generation quality and text-motion alignment. The mean values are reported in Table 1. The standard value is reported in Appendix F. (2) *Qualitative results.* We compare our method with MLD (Chen et al., 2023b) and T2M-GPT (Zhang et al., 2023). The comparison results show that our method has a stronger ability on generation quality (hand and body). For the “Flying Kick” case, MLD and T2M-GPT fail to generate desirable motions, but our method achieves it. For the second case, MLD fails to generate “forward” motion, and motions generated by T2M-GPT walk backward first and finally walk forward. In contrast, HumanTOMATO generates a vivid motion corresponding to textual descriptions.

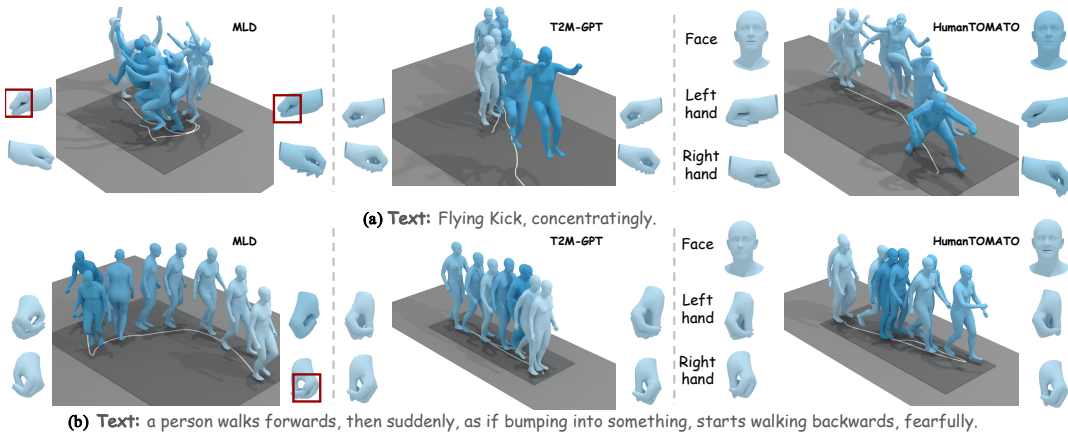


Figure 4: Qualitative comparison with baselines. HumanTOMATO supports face motion generation and outperforms MLD and T2M-GPT on hand motion generation and text-motion alignment.

3.4 ABALTION ON HIERARCHICAL DISCRETE REPRESENTATIONS (RQ2)

We compare the reconstruction result of our H²VQ with the Vanilla VQ (512 or 1024 codebook size) and RVQ methods on Motion-X and GRAB (Motion-X subset), which are shown in Table 2. Following the commonly used evaluation protocols on motion reconstruction, we take the MPJPE metric (Gower, 1975; Lin et al., 2023a; Chen et al., 2023b) to evaluate the reconstruction performance. As shown in Table 2, increasing the codebook size naïvely is almost in vain. The hierarchical modeling strategy improves the reconstruction performance significantly when learning informative low-dimensional representations. Moreover, our H²VQ is better than RVQ in reconstructing whole-body motions, with gains mainly coming from the modeling of body and hand discrete codes explicitly. When verifying the key insight of our hierarchical modeling on body-only datasets, in contrast to HumanML3D only including body-part motions, we compare the Vinilla VQ-VAE with the RVQ technique to verify our motivation. The results are shown in Appendix G. More evaluation metrics on PA-MPJPE and Acceleration error (Accel.) are also available in Appendix G.

3.5 TEXT-MOTION RETRIEVAL MODEL AS A PRIOR (RQ3)

Here, we evaluate our core design of introducing a pre-trained text-motion retrieval model as a prior. Ablation results in Table 3 show that our introduced motion-aware prior benefits the alignment

	Motion-X			GRAB			HumanML3D
	All↓	Body↓	Hand↓	All↓	Body↓	Hand↓	Body↓
Vanilla VQ (512)	140.66	92.197	46.4517	78.228	38.285	31.480	77.209
Vanilla VQ (1024)	139.33	91.768	46.399	76.013	37.340	29.887	71.335
RVQ	110.94	73.974	40.011	62.938	31.124	27.283	63.051
H ² VQ	92.966	62.34	37.1957	46.742	24.327	24.588	-

Table 2: Comparison of the motion reconstruction errors (MPJPE in mm) of different quantization methods on Motion-X, GRAB, and HumanML3D. Our H²VQ shows significant improvements.

embedding supervision	FID↓	TMR-R-Precision ⁽²⁵⁶⁾			R-Precision ⁽³²⁾			TMR-Matching-score↓	Matching-score↓
		Top1↑	Top2↑	Top3↑	Top1↑	Top2↑	Top3↑		
GT	0.002	0.500	0.708	0.814	0.407	0.578	0.673	0.768	2.888
CLIP ✗	1.086	0.405	0.588	0.695	0.345	0.490	0.573	0.844	3.917
TMR ✗	1.290	0.416	0.596	0.699	0.395	0.550	0.637	0.815	3.950
TMR ✓	1.174	0.416	0.603	0.703	0.399	0.555	0.638	0.809	3.894

Table 3: Ablation on a pre-trained text-motion-aligned model for motion generation on Motion-X. Both TMR embedding and text-motion alignment supervision help generate text-aligned motions.

between the generated motions and text. Visualization results in Appendix H show that our key design helps capture the motion dynamic clues better on sequentiality, directions, and dynamics.

3.6 ANALYSIS ON EVALUATION METRICS (RQ4)

We answer RQ4 from two aspects. (1) **Our TMR-R-Precision^(B) and TMR-Matching-score^(B) metrics are more accurate than the R-Precision^(B) and Matching-score metrics (Guo et al., 2022).** As shown in Figure 5, our TMR (in blue) shows stronger retrieval ability than Guo et al. (2022)’s retriever (in red) on both $B = 32$ and $B = 256$ settings. Moreover, Guo et al. (2022)’s retriever shows a larger retrieval gap than TMR when changing $B = 32$ to $B = 256$. Therefore, TMR can evaluate text-motion alignment more accurately than Guo et al. (2022). (2) **$B = 256$ is a more challenging retrieval setting than the $B = 32$ setting.** Retrieving text from motion in 32 text candidates is much easier than 256 candidates. As shown in Figure 5, when changing $B = 32$ to $B = 256$, the retrieval accuracy of both retrievers declines due to the increased size of the retrieval set, which makes the evaluation protocols more challenging. Overall, with a higher upper limit of retrieval capabilities, TMR-R-Precision⁽²⁵⁶⁾ can better evaluate the performance of different methods on text-motion alignment. Additionally, TMR-R-Precision^(B) and TMR-Matching-score are also more accurate and challenging metrics on the body-only dataset (HumanML3D). More details and numerical comparisons are in Appendix I.

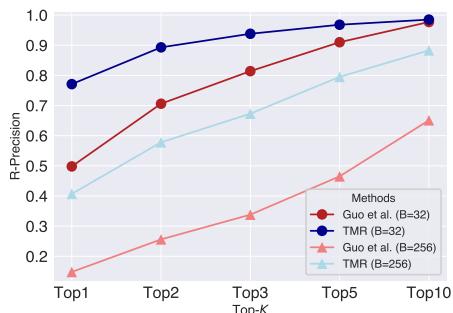


Figure 5: Comparison with existing metrics on Motion-X. Existing evaluation metrics (Guo et al., 2022) are illustrated in red, and ours are in green. The $B = 32$ and $B = 256$ settings for retrieval are denoted as “-●-” and “-▲-” respectively.

4 CONCLUSION

This work studies the problem of text-driven whole-body motion generation. We carefully clarify the existing challenges in generating vivid text-aligned whole-body motion on motion reconstruction and text-motion alignment. To tackle the challenges, two main technical contributions are proposed: (1) a Holistic Hierarchical VQ-VAE (H²VQ) and a Hierarchical-GPT for fine-grained body and hand motion reconstruction and generation, and (2) a pre-trained text-motion-alignment model to help generate text-aligned motion. We conduct comprehensive experiments to verify the superiority and effectiveness of the proposed solution on Motion-X and HumanML3D datasets. Experimental results show that HumanTOMATO can generate vivid text-aligned whole-body motion. The broader impact and limitation are discussed in Appendix J.

REFERENCES

- Kfir Aberman, Peizhuo Li, Dani Lischinski, Olga Sorkine-Hornung, Daniel Cohen-Or, and Baoquan Chen. Skeleton-aware networks for deep motion retargeting. *TOG*, 39(4):62, 2020.
- Hyemin Ahn, Timothy Ha, Yunho Choi, Hwiyeon Yoo, and Songhwai Oh. Text2action: Generative adversarial synthesis from language to action. In *ICRA*, 2018.
- Chaitanya Ahuja and Louis-Philippe Morency. Language2pose: Natural language grounded pose forecasting. In *3DV*, 2019.
- Tenglong Ao, Qingzhe Gao, Yuke Lou, Baoquan Chen, and Libin Liu. Rhythmic gesticulator: Rhythm-aware co-speech gesture synthesis with hierarchical neural embeddings. *ACM TOG*, 41(6):1–19, 2022.
- C.F. Barnes, S.A. Rizvi, and N.M. Nasrabadi. Advances in residual vector quantization: a review. *IEEE TIP*, 5(2):226–262, 1996. doi: 10.1109/83.480761.
- Yujun Cai, Yiwei Wang, Yiheng Zhu, Tat-Jen Cham, Jianfei Cai, Junsong Yuan, Jun Liu, Chuanxia Zheng, Sijie Yan, Henghui Ding, et al. A unified 3d human motion synthesis model via conditional variational auto-encoder. In *ICCV*, 2021.
- Ling-Hao Chen, Jiawei Zhang, Yewen Li, Yiren Pang, Xiaobo Xia, and Tongliang Liu. Humanmac: Masked motion completion for human motion prediction. *ICCV*, 2023a.
- Xin Chen, Biao Jiang, Wen Liu, Zilong Huang, Bin Fu, Tao Chen, Jingyi Yu, and Gang Yu. Executing your commands via motion diffusion in latent space. *CVPR*, 2023b.
- Jade Copet, Felix Kreuk, Itai Gat, Tal Remez, David Kant, Gabriel Synnaeve, Yossi Adi, and Alexandre Défossez. Simple and controllable music generation. *arXiv preprint arXiv:2306.05284*, 2023.
- Rishabh Dabral, Muhammad Hamza Mughal, Vladislav Golyanik, and Christian Theobalt. Mofusion: A framework for denoising-diffusion-based motion synthesis. In *CVPR*, pp. 9760–9770, 2023.
- Alexandre Défossez, Jade Copet, Gabriel Synnaeve, and Yossi Adi. High fidelity neural audio compression. *arXiv preprint arXiv:2210.13438*, 2022.
- Luciano Floridi and Massimo Chiriatti. Gpt-3: Its nature, scope, limits, and consequences. *Minds and Machines*, 2020.
- Anindita Ghosh, Noshaba Cheema, Cennet Oguz, Christian Theobalt, and Philipp Slusallek. Synthesis of compositional animations from textual descriptions. In *ICCV*, 2021.
- John C Gower. Generalized procrustes analysis. *Psychometrika*, 40:33–51, 1975.
- Chuan Guo, Shihao Zou, Xinxin Zuo, Sen Wang, Wei Ji, Xingyu Li, and Li Cheng. Generating diverse and natural 3d human motions from text. In *CVPR*, 2022.
- Ikhsanul Habibie, Weipeng Xu, Dushyant Mehta, Lingjie Liu, Hans-Peter Seidel, Gerard Pons-Moll, Mohamed Elgharib, and Christian Theobalt. Learning speech-driven 3d conversational gestures from video. In *ACM IVA*, pp. 101–108, 2021.
- Fangzhou Hong, Mingyuan Zhang, Liang Pan, Zhongang Cai, Lei Yang, and Ziwei Liu. Avatarclip: Zero-shot text-driven generation and animation of 3d avatars. *ACM SIGGRAPH*, 2022.
- Biao Jiang, Xin Chen, Wen Liu, Jingyi Yu, Gang Yu, and Tao Chen. Motiongpt: Human motion as a foreign language. In *NeurIPS*, 2023.
- Jihoon Kim, Jiseob Kim, and Sungjoon Choi. Flame: Free-form language-based motion synthesis & editing. In *AAAI*, volume 37, pp. 8255–8263, 2023.
- Diederik P Kingma and Max Welling. Auto-encoding variational bayes. In *ICLR*, 2013.
- Taeryung Lee, Gyeongsik Moon, and Kyoung Mu Lee. Multiact: Long-term 3d human motion generation from multiple action labels. In *AAAI*, volume 37, pp. 1231–1239, 2023.

- He Li, Shiyu Zhang, Xuejiao Li, Liangcai Su, Hongjie Huang, Duo Jin, Linghao Chen, Jianbin Huang, and Jaesoo Yoo. Detectornet: Transformer-enhanced spatial temporal graph neural network for traffic prediction. In *ACM SIGSPATIAL*, pp. 133–136, 2021a.
- Jiefeng Li, Chao Xu, Zhicun Chen, Siyuan Bian, Lixin Yang, and Cewu Lu. Hybrik: A hybrid analytical-neural inverse kinematics solution for 3d human pose and shape estimation. In *CVPR*, pp. 3383–3393, 2021b.
- Ronghui Li, Junfan Zhao, Yachao Zhang, Mingyang Su, Zeping Ren, Han Zhang, Yansong Tang, and Xiu Li. Finedance: A fine-grained choreography dataset for 3d full body dance generation. In *ICCV*, pp. 10234–10243, 2023a.
- Shikun Li, Xiaobo Xia, Shiming Ge, and Tongliang Liu. Selective-supervised contrastive learning with noisy labels. In *CVPR*, pp. 316–325, 2022.
- Shuai Li, Sisi Zhuang, Wenfeng Song, Xinyu Zhang, Hejia Chen, and Aimin Hao. Sequential texts driven cohesive motions synthesis with natural transitions. In *ICCV*, pp. 9498–9508, October 2023b.
- Jing Lin, Ailing Zeng, Shunlin Lu, Yuanhao Cai, Ruimao Zhang, Haoqian Wang, and Lei Zhang. Motion-x: A large-scale 3d expressive whole-body human motion dataset. *NeurIPS*, 2023a.
- Jing Lin, Ailing Zeng, Haoqian Wang, Lei Zhang, and Yu Li. One-stage 3d whole-body mesh recovery with component aware transformer. In *CVPR*, pp. 21159–21168, 2023b.
- Junfan Lin, Jianlong Chang, Lingbo Liu, Guanbin Li, Liang Lin, Qi Tian, and Chang-wen Chen. Being comes from not-being: Open-vocabulary text-to-motion generation with wordless training. In *CVPR*, pp. 23222–23231, 2023c.
- Haiyang Liu, Zihao Zhu, Naoya Iwamoto, Yichen Peng, Zhengqing Li, You Zhou, Elif Bozkurt, and Bo Zheng. Beat: A large-scale semantic and emotional multi-modal dataset for conversational gestures synthesis. In *ECCV*, pp. 612–630. Springer, 2022.
- Jun Liu, Amir Shahroudy, Mauricio Perez, Gang Wang, Ling-Yu Duan, and Alex C Kot. Ntu rgb+d 120: A large-scale benchmark for 3d human activity understanding. *TPAMI*, 2019.
- Ilya Loshchilov and Frank Hutter. Decoupled weight decay regularization. *ICLR*, 2019.
- Qiuqing Lu, Yipeng Zhang, Mingjian Lu, and Vwani Roychowdhury. Action-conditioned on-demand motion generation. In *ACM MM*, pp. 2249–2257, 2022.
- Thomas Lucas, Fabien Baradel, Philippe Weinzaepfel, and Grégory Rogez. Posegpt: Quantization-based 3d human motion generation and forecasting. In *ECCV*, pp. 417–435. Springer, 2022.
- Naureen Mahmood, Nima Ghorbani, Nikolaus F Troje, Gerard Pons-Moll, and Michael J Black. Amass: Archive of motion capture as surface shapes. In *ICCV*, 2019.
- Aaron van den Oord, Yazhe Li, and Oriol Vinyals. Representation learning with contrastive predictive coding. *arXiv preprint arXiv:1807.03748*, 2018.
- Georgios Pavlakos, Vasileios Choutas, Nima Ghorbani, Timo Bolkart, Ahmed AA Osman, Dimitrios Tzionas, and Michael J Black. Expressive body capture: 3d hands, face, and body from a single image. In *CVPR*, 2019.
- Mathis Petrovich, Michael J Black, and Gül Varol. Temos: Generating diverse human motions from textual descriptions. In *ECCV*, 2022.
- Mathis Petrovich, Michael J Black, and Gül Varol. Tmr: Text-to-motion retrieval using contrastive 3d human motion synthesis. *ICCV*, 2023.
- Matthias Plappert, Christian Mandery, and Tamim Asfour. The kit motion-language dataset. *Big data*, 4(4):236–252, 2016.
- Abhinanda R Punnakkal, Arjun Chandrasekaran, Nikos Athanasiou, Alejandra Quiros-Ramirez, and Michael J Black. Babel: bodies, action and behavior with english labels. In *CVPR*, 2021.

- Alec Radford, Jong Wook Kim, Chris Hallacy, Aditya Ramesh, Gabriel Goh, Sandhini Agarwal, Girish Sastry, Amanda Askell, Pamela Mishkin, Jack Clark, et al. Learning transferable visual models from natural language supervision. In *ICML*, 2021.
- Colin Raffel, Noam Shazeer, Adam Roberts, Katherine Lee, Sharan Narang, Michael Matena, Yanqi Zhou, Wei Li, and Peter J Liu. Exploring the limits of transfer learning with a unified text-to-text transformer. *JMLR*, 21(1):5485–5551, 2020.
- Ali Razavi, Aaron Van den Oord, and Oriol Vinyals. Generating diverse high-fidelity images with vq-vae-2. *NeurIPS*, 32, 2019.
- Nils Reimers and Iryna Gurevych. Sentence-bert: Sentence embeddings using siamese bert-networks. In *EMNLP-IJCNLP*, pp. 3982–3992, 2019.
- Robin Rombach, Andreas Blattmann, Dominik Lorenz, Patrick Esser, and Björn Ommer. High-resolution image synthesis with latent diffusion models. In *CVPR*, pp. 10684–10695, 2022.
- Victor Sanh, Lysandre Debut, Julien Chaumond, and Thomas Wolf. Distilbert, a distilled version of bert: smaller, faster, cheaper and lighter. *arXiv preprint arXiv:1910.01108*, 2019.
- Li Siyao, Weijiang Yu, Tianpei Gu, Chunze Lin, Quan Wang, Chen Qian, Chen Change Loy, and Ziwei Liu. Bailando: 3d dance generation by actor-critic gpt with choreographic memory. In *CVPR*, pp. 11050–11059, 2022.
- Kaitao Song, Xu Tan, Tao Qin, Jianfeng Lu, and Tie-Yan Liu. Mpnet: Masked and permuted pre-training for language understanding. *NeurIPS*, 33:16857–16867, 2020.
- Omid Taheri, Nima Ghorbani, Michael J Black, and Dimitrios Tzionas. Grab: A dataset of whole-body human grasping of objects. In *ECCV*, 2020.
- Guy Tevet, Brian Gordon, Amir Hertz, Amit H Bermano, and Daniel Cohen-Or. Motionclip: Exposing human motion generation to clip space. In *ECCV*, 2022.
- Guy Tevet, Sigal Raab, Brian Gordon, Yonatan Shafir, Amit H Bermano, and Daniel Cohen-Or. Human motion diffusion model. *ICLR*, 2023.
- Jonathan Tseng, Rodrigo Castellon, and Karen Liu. Edge: Editable dance generation from music. In *CVPR*, pp. 448–458, 2023.
- Aaron Van Den Oord, Oriol Vinyals, et al. Neural discrete representation learning. *NeurIPS*, 30, 2017.
- Ashish Vaswani, Noam Shazeer, Niki Parmar, Jakob Uszkoreit, Llion Jones, Aidan N Gomez, Łukasz Kaiser, and Illia Polosukhin. Attention is all you need. *NeurIPS*, 30, 2017.
- Duomin Wang, Yu Deng, Zixin Yin, Heung-Yeung Shum, and Baoyuan Wang. Progressive disentangled representation learning for fine-grained controllable talking head synthesis. In *CVPR*, pp. 17979–17989, 2023a.
- Jingbo Wang, Yu Rong, Jingyuan Liu, Sijie Yan, Dahua Lin, and Bo Dai. Towards diverse and natural scene-aware 3d human motion synthesis. In *CVPR*, pp. 20460–20469, 2022a.
- Yinhui Wang, Jiwen Yu, and Jian Zhang. Zero-shot image restoration using denoising diffusion null-space model. *ICLR*, 2023b.
- Zan Wang, Yixin Chen, Tengyu Liu, Yixin Zhu, Wei Liang, and Siyuan Huang. Humanise: Language-conditioned human motion generation in 3d scenes. *NeurIPS*, 35:14959–14971, 2022b.
- Zhenyi Wang, Ping Yu, Yang Zhao, Ruiyi Zhang, Yufan Zhou, Junsong Yuan, and Changyou Chen. Learning diverse stochastic human-action generators by learning smooth latent transitions. In *AAAI*, 2020.
- Xiaobo Xia, Tongliang Liu, Nannan Wang, Bo Han, Chen Gong, Gang Niu, and Masashi Sugiyama. Are anchor points really indispensable in label-noise learning? *NeurIPS*, 32, 2019.

- Xiaobo Xia, Tongliang Liu, Bo Han, Nannan Wang, Mingming Gong, Haifeng Liu, Gang Niu, Dacheng Tao, and Masashi Sugiyama. Part-dependent label noise: Towards instance-dependent label noise. *NeurIPS*, 33:7597–7610, 2020.
- Sirui Xu, Yu-Xiong Wang, and Liang-Yan Gui. Diverse human motion prediction guided by multi-level spatial-temporal anchors. In *ECCV*, pp. 251–269. Springer, 2022.
- Sirui Xu, Zhengyuan Li, Yu-Xiong Wang, and Liang-Yan Gui. Interdiff: Generating 3d human-object interactions with physics-informed diffusion. *ICCV*, 2023a.
- Sirui Xu, Yu-Xiong Wang, and Liang-Yan Gui. Stochastic multi-person 3d motion forecasting. In *ICLR*, 2023b.
- Sijie Yan, Zhizhong Li, Yuanjun Xiong, Huahan Yan, and Dahua Lin. Convolutional sequence generation for skeleton-based action synthesis. In *ICCV*, 2019.
- Jie Yang, Ailing Zeng, Shilong Liu, Feng Li, Ruimao Zhang, and Lei Zhang. Explicit box detection unifies end-to-end multi-person pose estimation. In *ICLR*, 2023.
- Heyuan Yao, Zhenhua Song, Yuyang Zhou, Tenglong Ao, Baoquan Chen, and Libin Liu. Moconvq: Unified physics-based motion control via scalable discrete representations. *arXiv preprint arXiv:2310.10198*, 2023.
- Hongwei Yi, Hualin Liang, Yifei Liu, Qiong Cao, Yandong Wen, Timo Bolkart, Dacheng Tao, and Michael J Black. Generating holistic 3d human motion from speech. In *CVPR*, 2023.
- Ping Yu, Yang Zhao, Chunyuan Li, Junsong Yuan, and Changyou Chen. Structure-aware human-action generation. In *ECCV*, 2020.
- Zhentao Yu, Zixin Yin, Deyu Zhou, Duomin Wang, Finn Wong, and Baoyuan Wang. Talking head generation with probabilistic audio-to-visual diffusion priors. In *ICCV*, pp. 7645–7655, 2023.
- Ye Yuan, Jiaming Song, Umar Iqbal, Arash Vahdat, and Jan Kautz. Physdiff: Physics-guided human motion diffusion model. *ICCV*, 2023.
- Neil Zeghidour, Alejandro Luebs, Ahmed Omran, Jan Skoglund, and Marco Tagliasacchi. Soundstream: An end-to-end neural audio codec. *TASLP*, 30:495–507, 2021.
- Ailing Zeng, Lei Yang, Xuan Ju, Jiefeng Li, Jianyi Wang, and Qiang Xu. Smoothnet: A plug-and-play network for refining human poses in videos. In *ECCV*, pp. 625–642. Springer, 2022.
- Jianrong Zhang, Yangsong Zhang, Xiaodong Cun, Shaoli Huang, Yong Zhang, Hongwei Zhao, Hongtao Lu, and Xi Shen. T2m-gpt: Generating human motion from textual descriptions with discrete representations. *CVPR*, 2023.
- Mingyuan Zhang, Zhongang Cai, Liang Pan, Fangzhou Hong, Xinying Guo, Lei Yang, and Ziwei Liu. Motiondiffuse: Text-driven human motion generation with diffusion model. *arXiv preprint arXiv:2208.15001*, 2022.
- Yan Zhang, Michael J Black, and Siyu Tang. Perpetual motion: Generating unbounded human motion. *arXiv preprint arXiv:2007.13886*, 2020.
- Rui Zhao, Hui Su, and Qiang Ji. Bayesian adversarial human motion synthesis. In *CVPR*, 2020.
- Zixiang Zhou and Baoyuan Wang. Ude: A unified driving engine for human motion generation. In *CVPR*, pp. 5632–5641, 2023.

Appendix:

HumanTOMATO: Text-aligned Whole-body Motion Generation

A RELATED WORK

Human Motion Generation. Generating human motions can be divided into two main types according to inputs: motion synthesis (1) without any conditions (Yan et al., 2019; Zhao et al., 2020; Zhang et al., 2020; Cai et al., 2021) and (2) with some given conditions, such as text, audio, music, and interactive scenes (Ahn et al., 2018; Petrovich et al., 2022; Zhang et al., 2022; Chen et al., 2023b; Guo et al., 2022; Ahuja & Morency, 2019; Ghosh et al., 2021; Zhang et al., 2023; Lee et al., 2023; Yi et al., 2023; Wang et al., 2022a; Zhou & Wang, 2023; Wang et al., 2022b; Xu et al., 2022; Tseng et al., 2023; Siyao et al., 2022; Liu et al., 2022; Xu et al., 2023b; Dabral et al., 2023). The second type will be more challenging and applicable due to either extracting and understanding motion and conditions or cross-modality alignment. To generate diverse, natural, high-quality human motions, many generative models have been explored by Wang et al. (2020); Yu et al. (2020); Zhang et al. (2023). Recently, diffusion-based models significantly improved the motion generation performance and diversity (Chen et al., 2023b; Tevet et al., 2023; Zhang et al., 2022; Wang et al., 2023b; Chen et al., 2023a; Xu et al., 2023a; Li et al., 2023a;b) with stable training. However, as human motion is a kind of high-dimensional spatio-temporal signal (Li et al., 2021a), these methods are still hard to tackle the motion data easily. Chen et al. (2023b); Zhang et al. (2023) learn low-dimensional motion latent in an encoding-decoding fashion, like VAE and VQ-VAE, in the first stage. Then, text-aligned motion latent representations could be easier to learn in the second stage. For holistic human motion generation with facial expressions and hand gestures, co-speech expression generation and gesture generation from human speech is also an arising topic in this area (Habibie et al., 2021; Yi et al., 2023). Specifically, TalkSHOW (Yi et al., 2023) takes the first attempt for face, hand, and body motion modeling via separate models since the facial expressions (*e.g.*, lip movement) are strongly correlated with the speech signals (Yu et al., 2023; Wang et al., 2023a), but the body and gesture motions are many-to-many mappings. Bearing the difficulties in jointly modeling the whole-body motions and the lack of whole-body data, there are no existing methods to explore text-driven whole-body motion generation.

Text-driven Motion Generation. Text plays an important role in controlling human motion generation since it can describe the actions, directions, and dynamic body-part clues via a natural interaction way. Based on existing action recognition and motion capture datasets (Plappert et al., 2016; Mahmood et al., 2019; Liu et al., 2019; Punnakkal et al., 2021; Guo et al., 2022), text-driven motion generation has achieved rapid progress in recent years. The input text went from the original single-action category to multiple actions and arbitrary natural language (Ahn et al., 2018; Lee et al., 2023; Lu et al., 2022; Petrovich et al., 2022; Kim et al., 2023). The generated motions also range from upper-body motions to full-body motions (additionally with global trajectories and lower-body motions) and from short-time actions to long-term motions (Ahuja & Morency, 2019; Chen et al., 2023b; Zhang et al., 2023). Early attempts (Tevet et al., 2022; Guo et al., 2022) heavily rely on the given motion-text datasets, making the generated motion hard to generalize. For open-vocabulary motion generation, some works try to introduce large-scale pre-trained models (*e.g.*, CLIP (Radford et al., 2021), and LLMs (Floridi & Chiriatti, 2020)) to make the text encoding powerful (Lucas et al., 2022; Jiang et al., 2023; Tevet et al., 2022; Hong et al., 2022; Lin et al., 2023c). However, existing methods suffer from two main issues. First, text-driven holistic motion generation is under-explored, while coherent hand gestures and facial expressions are essential to whole-body motions. Second, the distribution of motion is quite different from images, making CLIP prior weak in text-motion alignment, while LLMs only have textual priors. That is to say, previous efforts have not thoroughly explored motion-text alignment. Accordingly, modeling whole-body motion and exploring how to use motion-text-aligned priors are urgent for the community.

B IMPLEMENTATION DETAILS

B.1 MOTION REPRESENTATION

The raw motion representation consists of two parts (Aberman et al., 2020), static part (joints offsets) and dynamic part (joint movements) respectively. We further define motion generation tasks as generating diverse and vivid joint movements based on a uniform skeleton. We follow Guo et al. (2022) (i.e. H3D-Format) to randomly select a skeleton as a target skeleton, including body and hand joints, and retarget each motion sequence to it. As all motions share the same skeleton, in this way, we set the local joint offsets for all motions to be unchanged. As a pose can be decomposed as twist and swing (Li et al., 2021b), vanilla inverse kinematic (IK) algorithms will ignore the twist rotation, which will lead to the wrong supervision of joint movements. To verify whether rotation regularization helps motion generation and reconstruction, we take motion reconstruction as a pre-text task. For motion reconstruction, we take a transformer-based VAE (Chen et al., 2023b) and convolution-based VQ-VAE (Zhang et al., 2023) as the architecture to evaluate the motion reconstruction performance on HumanML3D. As shown in Table 4, motion without rotation information reduces the reconstruction error. Besides, the results in Table 4 show that velocity is beneficial to motion reconstruction.

As discussed in the main paper (Section 3.2), for body-hand motion representations, we take the H3D-Format (Guo et al., 2022) as a basis and expand the body-only representation to holistic body-hand motion representation. Specifically, the i -th frame pose is defined by a tuple of root angular velocity ($\dot{r}^a \in \mathbb{R}$) along Y-axis, root linear velocities ($\dot{r}^x, \dot{r}^z \in \mathbb{R}$) on XZ-plane, root height $r^y \in \mathbb{R}$, local joints positions ($\mathbf{j}^p \in \mathbb{R}^{3N-1}$), and velocities ($\mathbf{j}^v \in \mathbb{R}^{3N}$), where N denotes the number of joints. For face motion representations, we follow Flame Format (Kim et al., 2023) and use $\mathbf{f} \in \mathbb{R}^{50}$ to represent the face expression. Thus, we represent the whole-body motion at frame i as $\mathbf{m}_i = \{\dot{r}^a, \dot{r}^x, \dot{r}^z, \dot{r}^y, \mathbf{j}^p, \mathbf{j}^v, \mathbf{f}\}$.

	Input Format	MPJPE	PA-MPJPE	ACCEL.
VAE	H3D-format	49.51	39.47	7.131
	w/o rotation, w/o velocity	51.43	39.47	7.27
	w/o rotation	46.84	36.16	6.603
VQ-VAE	H3D-format	78.24	45.77	8.757
	w/o rotation, w/o velocity	76.34	39.98	8.622
	w/o rotation	68.86	39.97	8.274

Table 4: Ablation study of different motion representations on the Humanml3D dataset.

B.2 IMPLEMENTATION DETAILS OF HIERARCHICAL MOTION VQ-VAE

We take Conv1d(\cdot) with skip connection as the basic module for both the body encoder and the hand encoder and downsample the feature from the body part by $2\times$ and the feature from the hand part by $4\times$, respectively. In detail, at each down-sampled timestamp, the number of body tokens is 2, and the number of hand tokens is 4. Therefore, we predict two body tokens at each down-sampled timestamp. The codebook size for both hand quantizer and body quantizer is set to 512×512 . That is to say, $K = 512$ and the dimension of each code is 512. We take the AdamW (Loshchilov & Hutter, 2019) as an optimizer with a fixed learning rate 1×10^{-4} , batch size of 256, and exponential moving constant $\lambda = 0.99$. The α in H^2VQ loss \mathcal{L} (Eqn. 3) is set as 0.02. The body-hand decoder upsamples the feature by $2\times$. All upsampling operation in the decoder is the nearest upsampling with a scaling factor of $2\times$. Training the H^2VQ takes about 8 hours on $4\times$ NVIDIA Tesla A100-80GB GPUs.

B.3 IMPLEMENTATION DETAILS OF THE HIERARCHICAL-GPT.

We employ 18 transformer layers with a dimension of 1024 and 16 heads. Since the design of different downsampling rates between two codebooks, we simply concat the tokens from pre-trained H^2VQ stage and set the maximum length of the code index sequence as 149.

Training. We combine the tokens from the hand codebook \mathcal{C}_1 and the body codebook \mathcal{C}_2 and feed them into the transformer, in which we employ a causal mask with $mask_{i,j} = -\infty \times \mathbf{1}(i <$

$j)+\mathbf{1}(i \geq j)$, where $\mathbf{1}(\cdot)$ is the indicator function, to prevent information leakage from the following tokens. We employ the CLIP-ViT-L-14 model and pre-trained TMR Text encoder as the text encoder to encode the text, respectively, and freeze them in training. All the trainings are conducted on $4 \times$ NVIDIA Tesla A100-80GB GPUs and cost 60 hours.

Inference. When performing inference, we feed the text encoder with raw texts and get the text embedding. Our Hierarchical-GPT predicts motion tokens in an auto-regressive fashion with the start token of text embedding. All our tests and inferences are conducted on $1 \times$ NVIDIA Tesla A100-80GB GPU.

B.4 FACIAL CVAE

As discussed in the main paper (Section 2.3), we take the cVAE (Petrovich et al., 2022) to generate text-driven facial motions. The facial VAE consists of three components. (1) A facial encoder. The Facial is a 6-layer transformer. The input facial motion is concatenated with a μ_F token and a Σ_F token. (2) A text encoder. The Facial is composed of a pre-trained DistilBERT (Sanh et al., 2019) and a 6-layer transformer. The input DistilBERT feature is concatenated with a μ_T token and a Σ_T token. (3) A facial decoder. The 6-layer transformer-based facial decoder generates facial motions from the z_F or z_T vector, which can be sampled from Gaussian distribution $\mathcal{N}(\mu_F, \Sigma_F)$ or $\mathcal{N}(\mu_T, \Sigma_T)$ via re-parameterizing trick (Kingma & Welling, 2013). The training loss consists of three components. (1) facial motion reconstruction loss:

$$\mathcal{L}_{rec} = \text{SmoothL1}(\mathbf{m}^F, \hat{\mathbf{m}}^F),$$

where $\mathbf{m}^F, \hat{\mathbf{m}}^F$ are facial motions and reconstructed facial motions and $\text{SmoothL1}(\cdot)$ is the SmoothL1-Loss. (2) KL Loss:

$$\begin{aligned} \mathcal{L}_{KL} = & \text{KL}(\mathcal{N}(\mu_F, \Sigma_F), \mathcal{N}(\mathbf{0}, \mathbf{I})) + \text{KL}(\mathcal{N}(\mu_T, \Sigma_T), \mathcal{N}(\mathbf{0}, \mathbf{I})) \\ & + \text{KL}(\mathcal{N}(\mu_F, \Sigma_F), \mathcal{N}(\mu_T, \Sigma_T)) + \text{KL}(\mathcal{N}(\mu_T, \Sigma_T), \mathcal{N}(\mu_F, \Sigma_F)), \end{aligned}$$

where $\text{KL}(\cdot)$ is the Kullback-Leibler divergence function and $\mathcal{N}(\mathbf{0}, \mathbf{I})$ is the Gaussian distribution. (3) Cross-modal embedding similarity loss:

$$\mathcal{L}_E = \text{SmoothL1}(z_F, z_T).$$

The overall training loss is $\mathcal{L} = \mathcal{L}_{rec} + \lambda_1 \mathcal{L}_{KL} + \lambda_2 \mathcal{L}_E$, where $\lambda_1 = \lambda_2 = 1 \times 10^{-5}$. In the inference stage, the text encoder encodes text embedding z_T first, and then feeds it into the facial decoder to obtain the facial motions.

C ALGORITHM FLOW OF H²VQ AND COMPARISON WITH RESIDUAL VECTOR QUANTIZATION

C.1 TRAINING AND INFERENCE OF H²VQ

In the main paper, we introduce the training and inference details in Section 2.2. For reading convenience, we provide the training and inference procedure of our Holistic Hierarchical VQ-VAE (H²VQ-VAE) in Algorithm 1 and Algorithm 2.

Algorithm 1: Training procedure of Holistic Hierarchical VQ-VAE (H²VQ-VAE)

Input: The initialized hand codebook \mathcal{C}_1 , body codebook \mathcal{C}_2 , hand quantizer $\mathcal{Q}^H(\cdot; \mathcal{C}^H)$, body quantizer $\mathcal{Q}^B(\cdot; \mathcal{C}^B)$ ($|\mathcal{C}^H| = |\mathcal{C}^B| = K$), H²VQ-VAE, the input motion \mathbf{m} , the optimization iterations I_{max} .

Output: The optimized H²VQ-VAE network Θ , codebooks $\mathcal{C}^H, \mathcal{C}^B$.

for $I = 0, 1, \dots, I_{max}$ **do**

$\mathbf{z}^H = \text{Enc}_H(\mathbf{m}^H);$
 $\mathbf{z}^B = \text{Enc}_B(\mathbf{m}^B);$
 $\hat{\mathbf{z}}^H = \mathcal{Q}^H(\mathbf{z}^H; \mathcal{C}^H);$
 $\hat{\mathbf{z}}^B = \mathcal{Q}^B(\text{Conv1d}(\text{Concat}(\text{Transform}(\hat{\mathbf{z}}^H), \hat{\mathbf{z}}^B)); \mathcal{C}^B);$
 $\hat{\mathbf{m}} = \text{Dec}(\hat{\mathbf{z}}^B, \hat{\mathbf{z}}^H);$
 $\Theta = \Theta - \nabla_{\Theta} \|\mathbf{m} - \text{Dec}(\hat{\mathbf{m}})\|_2^2 + \alpha (\|\mathbf{z}^H - \text{sg}(\hat{\mathbf{z}}^H)\|_2^2 + \|\mathbf{z}^B - \text{sg}(\hat{\mathbf{z}}^B)\|_2^2);$
 Optimize two codebooks $\mathcal{C}^H, \mathcal{C}^B$ via EMA and Code Reset;

return H²VQ-VAE network Θ .

Algorithm 2: Inference procedure of Holistic Hierarchical VQ-VAE (H²VQ-VAE)

Input: The pre-trained H²VQ-VAE network Θ , body and hand code indices sequence

$\mathbf{I}^B = [\mathbf{I}_1^B, \mathbf{I}_2^B, \dots, \mathbf{I}_{L/r}^B, \text{End}]$ and $\mathbf{I}^H = [\mathbf{I}_1^H, \mathbf{I}_2^H, \dots, \mathbf{I}_{L/r}^H, \text{End}]$, codebook

$\mathcal{C}^H = \{k, \mathbf{e}_1(k)\}_{k \in [K]}, \mathcal{C}^B = \{k, \mathbf{e}_2(k)\}_{k \in [K]}.$

Output: the noise prediction network ϵ_{θ} .

$\hat{\mathbf{z}}^H \leftarrow \text{Query } \mathcal{C}^H \text{ with } \mathbf{I}^H;$

$\hat{\mathbf{z}}^B \leftarrow \text{Query } \mathcal{C}^B \text{ with } \mathbf{I}^B;$

return motion $\text{Dec}(\hat{\mathbf{z}}^B, \hat{\mathbf{z}}^H).$

C.2 COMPARISON WITH RESIDUAL VECTOR QUANTIZATION (RVQ)

As can be seen in Appendix C.1, our H²VQ consists of two codebooks \mathcal{C}^H and \mathcal{C}^B with size K . The intuitive design insight is that the space of our code combination is $\mathcal{O}(K^2)$. However, scaling the size of the codebook to $2K$ only has the vector space of size $\mathcal{O}(K)$. Therefore, our H²VQ enjoys the scaling of latent code size with low memory cost. An alternative way to scale the codebook size efficiently is the 2-level Residual Vector Quantization (RVQ) technique. As shown in Algorithm 3, RVQ quantized the residual error vectors recurrently in each level, which is also a hierarchical modeling strategy. However, RVQ does not model the hand and body motions explicitly, which makes it cannot reconstruct the whole-body motions better than H²VQ. For more details, please refer to Zeghidour et al. (2021). The experimental comparisons are in Appendix G.

Algorithm 3: Residual Vector Quantization (RVQ)

Input: The output of the encoder $\mathbf{z} = \text{Enc}(\mathbf{m})$, N_q -level quantizers $\mathcal{Q}_i(\cdot)$ ($i = 1, 2, \dots, N_q$).

Output: Quantized vector $\hat{\mathbf{z}}$.

$\hat{\mathbf{z}} = \mathbf{0};$

$\text{res} = \mathbf{z};$

for $i = 1, 2, \dots, N_q$ **do**

$\hat{\mathbf{z}} + = \mathcal{Q}_i(\text{res});$
 $\text{res} - = \mathcal{Q}_i(\text{res});$

return $\hat{\mathbf{z}}$.

D TRAINING DETAILS AND EVALUATION ON TEXT-MOTION RETRIEVAL PRE-TRAINING

In this section, we will detail the training details of the TMR model and evaluate our pre-trained retrieval model.

D.1 TRAIN DETAILS

Here, we detail the training procedure on how to train a text-whole-body-motion retrieval model. Recall a text-to-motion model, TEMOS (Petrovich et al., 2022), the VAE-based architecture consists of a motion encode, a text encoder, and a motion decoder. The training objective in TEMOS is the weighted sum of $\mathcal{L}_T = \mathcal{L}_{rec} + \lambda_{KL}\mathcal{L}_{KL} + \lambda_E\mathcal{L}_E$, where the three loss items are reconstruction loss, Kullback-Leibler (KL) divergence loss, and cross-modal embedding similarity loss respectively. Additionally, like Petrovich et al. (2023), we introduce an InfoNCE (Oord et al., 2018) loss term \mathcal{L}_{NCE} into the optimization objective for learning text-motion-aligned representations. The InfoNCE loss aims to align pairwise text-motion embeddings and pull the negative motion-text pairs in the batch away like Radford et al. (2021). Therefore, the final training objective is

$$\min \mathcal{L}_T + \lambda_{NCE}\mathcal{L}_{NCE},$$

where all hyper-parameters are $\lambda_{KL} = 1 \times 10^{-5}$, $\lambda_E = 1 \times 10^{-5}$, $\lambda_{NCE} = 1 \times 10^{-1}$ respectively.

Note that, in a batch, different motion samples might be similar or even repetitive. Therefore, we will filter the similar negative samples in the InfoNCE loss. In other words, two motions with similar text descriptions (similarity higher than 0.85) will not be treated as negative samples. Technically, a pre-trained language model will calculate the similarity between two text descriptions $s_{i,j} = \langle \mathbf{t}_i, \mathbf{t}_j \rangle$, where $\langle \cdot, \cdot \rangle$ denotes the cosine similarity. Different from Petrovich et al. (2023) choosing MPNet¹ (Song et al., 2020) as the pre-trained language model, we take the Sentence-BERT (aka sBERT²) (Reimers & Gurevych, 2019) as the pre-trained language model, which is more accurate than MPNet.

To compare the accuracy of evaluating the similarity among sentences, we present a case study composed of 10 sentence samples in Example 1.

Example 1 Here, we present the 10 sentence samples used for evaluating sBERT and MPNet.

```
[
  0: 'A human walking backwards.',
  1: 'A person is walking backwards.',
  2: 'Someone walks in a circle counterclockwise',
  3: 'A person walks a full counter-clockwise circle.',
  4: 'A human performs a tight 90° curve to the right.',
  5: 'A person walks a quarter circle clockwise with 4 steps.',
  6: 'human goes backwards starting with left',
  7: 'A person walks backwards.',
  8: 'a person walks in a circle to the left side.',
  9: 'trump'
]
```

We calculate the cosine similarity of these 10 sentences with sBERT and MPNet, respectively. As shown in Figure 6, sBERT reflects the sentence similarity more accurately than MPNet. For two sentences with very similar semantics, like 'A human walking backwards.' and 'A person is walking backwards.', the similarity provided by sBERT is 0.958, while MPNet is 0.893. For two sentences completely unrelated, like 'A human walking backwards.' and 'trump', the similarity provided by sBERT is 0.132, while MPNet is 0.758. In this case, the 'trump' example is not a motion description. sBERT clearly distinguishes it from other sentences, but MPNet cannot distinguish them significantly. Therefore, the sBERT is more discriminative than MPNet in negative filtering.

¹<https://huggingface.co/microsoft/mpnet-base>.

²<https://huggingface.co/sentence-transformers/all-MiniLM-L6-v2>.

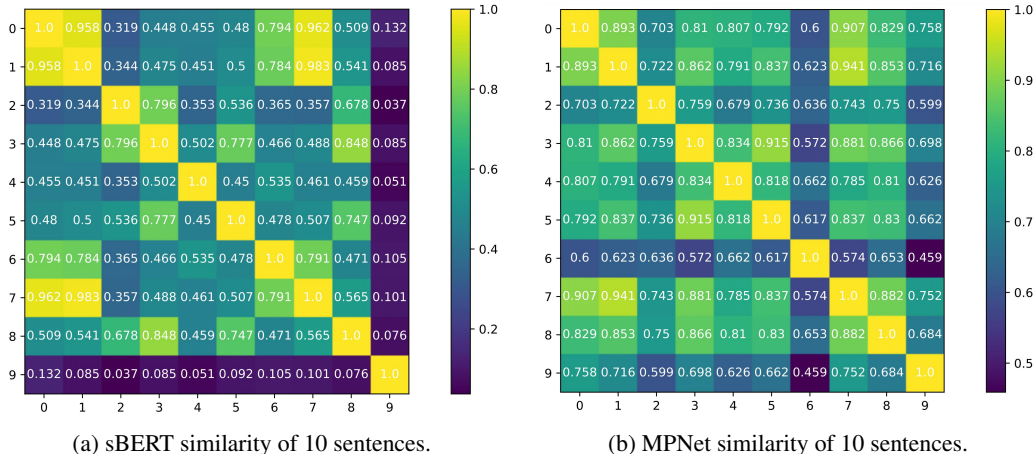


Figure 6: Sentences similarity comparison between the sBERT and MPNet .

D.2 EVALUATION OF THE RETRIEVAL MODEL

We take the Recall@ K as the main metric to evaluate the retrieval performance to evaluate the performance of the TMR model. We evaluate both motion-to-text (M2T) and text-to-motion (T2M) retrieval performance with four main protocols. (A) *Retrieving in the full test test*. (B) *Retrieving in the full test test with a sBERT-score threshold (set ϵ as 0.9)*. As some sentences have similar semantics, like “A man is walking straight.” and “The person walks forward.”, we treat these retrieval results as positive targets if the retrieved text has a sBERT similarity higher than $\epsilon = 0.9$ with GT text. (C) *Retrieving in the 256-size sub-test set*. The 256-size retrieving set consists of one GT result and 255 negative results. (D) *Retrieving in the 32-size sub-test set*. Similar to Protocol C, the 32-size retrieving set consists of one GT result and 31 negative results. The T2M and M2T retrieval evaluation results on Motion-X are shown in Table 5. The T2M and M2T retrieval evaluation results on HumanML3D are shown in Table 6. The comparison with other text-motion retrieval methods on the protocol (C) and protocol (D) is shown in Appendix I. **The retrieval web demo on both body-only and whole-body datasets will be public.**

	T2M					M2T				
	Recall@1	Recall@2	Recall@3	Recall@5	Recall@10	Recall@1	Recall@2	Recall@3	Recall@5	Recall@10
Protocol A	0.051	0.098	0.131	0.192	0.301	0.066	0.118	0.163	0.233	0.350
Protocol B	0.089	0.152	0.194	0.273	0.401	0.169	0.205	0.238	0.298	0.395
Protocol C	0.445	0.609	0.700	0.799	0.883	0.407	0.578	0.673	0.795	0.883
Protocol D	0.716	0.854	0.907	0.946	0.977	0.771	0.893	0.938	0.968	0.985

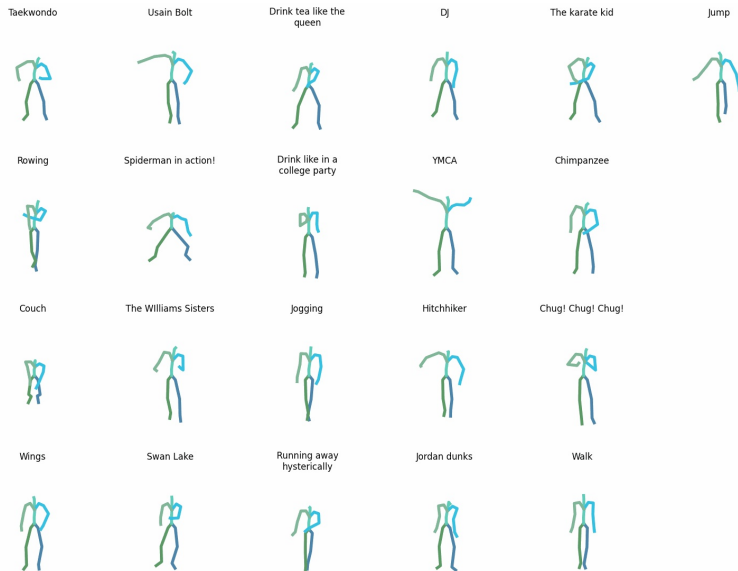
Table 5: Recall@ K (T2M and M2T) of GT motions and texts on the Motion-X dataset.

	T2M					M2T				
	Recall@1	Recall@2	Recall@3	Recall@5	Recall@10	Recall@1	Recall@2	Recall@3	Recall@5	Recall@10
Protocol A	0.065	0.117	0.155	0.227	0.339	0.057	0.106	0.144	0.205	0.322
Protocol B	0.204	0.282	0.326	0.404	0.510	0.102	0.151	0.199	0.263	0.373
Protocol C	0.359	0.523	0.630	0.729	0.842	0.365	0.527	0.625	0.731	0.838
Protocol D	0.774	0.896	0.937	0.968	0.985	0.711	0.853	0.905	0.947	0.977

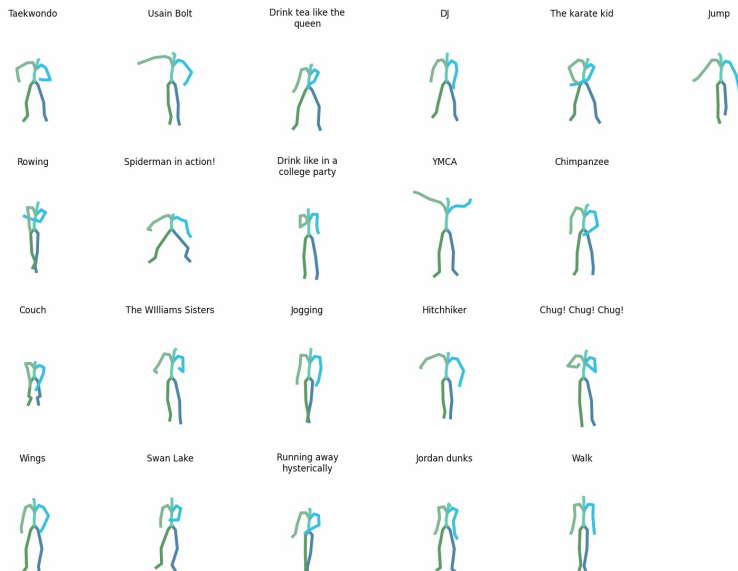
Table 6: Recall@ K (T2M and M2T) of GT motions and texts on the HumanML3D dataset.

E FAILURE CASES OF BASELINES

As discussed in Section 2.4, previous methods shown in Figure 3 will fail in some scenarios. We discuss the fashion of “Supervision by an image-text aligned prior explicitly” (Figure 3a) here. As there was no strong text-motion-aligned pre-trained model, MotionCLIP (Tevet et al., 2022) renders the generated motions as images and then supervises the alignment between text and rendered images with the CLIP model. This supervision will cause the generated motion to be *over-smoothing*, even *stillness*. We show some over-smoothing cases^{3,4} of MotionCLIP on here. As shown in Figure 7, there is almost no change at all between the first frame (Figure 7a) and the final frame (Figure 7b) of motion.



(a) The first frame of motion.



(b) The final frame of motion.

Figure 7: Visualization of MotionCLIP generated results. The first frame and the final frame of motions are shown in the figure.

³<https://github.com/GuyTevet/MotionCLIP/issues/5>.

⁴<https://github.com/GuyTevet/MotionCLIP/issues/15>.

F MORE DETAILS ON MAIN RESULTS (RQ1)

F.1 QUANTITATIVE COMPARISON

In the main paper, we report the metrics of our HumanTOMATO and related baselines in Table 1. We repeat the evaluation 5 times and report the mean \pm std results in Table 7 and Table 8. Experimental results show our strength than baseline on generation quality, text-motion alignment, and diversity.

	FID \downarrow	TMR-R-Precision ⁽²⁵⁶⁾			R-Precision ⁽³²⁾		
		Top1 \uparrow	Top2 \uparrow	Top3 \uparrow	Top1 \uparrow	Top2 \uparrow	Top3 \uparrow
GT	-	0.500 \pm 0.002	0.708 \pm 0.002	0.814 \pm 0.002	0.407 \pm 0.003	0.578 \pm 0.004	0.673 \pm 0.003
T2M-GPT	1.366 \pm 0.059	0.368 \pm 0.005	0.553 \pm 0.003	0.655 \pm 0.007	0.310 \pm 0.001	0.446 \pm 0.007	0.527 \pm 0.014
MDM	3.800 \pm 0.020	0.352 \pm 0.003	0.547 \pm 0.002	0.634 \pm 0.004	0.310 \pm 0.004	0.430 \pm 0.007	0.530 \pm 0.014
MLD	3.407 \pm 0.020	0.385 \pm 0.002	0.571 \pm 0.001	0.683 \pm 0.001	0.333 \pm 0.004	0.477 \pm 0.003	0.561 \pm 0.001
HumanTOMATO	1.174\pm0.015	0.416\pm0.009	0.603\pm0.007	0.703\pm0.007	0.399\pm0.000	0.555\pm0.005	0.638\pm0.004

Table 7: Quantitative Comparison on the Motion-X dataset (FID, TMR-R-Precision⁽²⁵⁶⁾, and R-Precision⁽³²⁾ metrics).

	TMR-Matching Score \downarrow	Matching Score \downarrow	MModality \uparrow	Diversity \uparrow
GT	0.768 \pm 0.000	2.888 \pm 0.006	-	11.087 \pm 0.271
T2M-GPT	0.881 \pm 0.004	4.316 \pm 0.053	2.356 \pm 0.093	10.753 \pm 0.063
MDM	0.840 \pm 0.004	4.050 \pm 0.023	2.530\pm0.041	11.400\pm0.370
MLD	0.883 \pm 0.002	3.901 \pm 0.011	2.448 \pm 0.034	10.420 \pm 0.234
HumanTOMATO	0.809\pm0.002	3.894\pm0.008	1.732 \pm 0.194	10.812 \pm 0.034

Table 8: Quantitative Comparison on the Motion-X dataset (TMR-Matching Score, Matching Score, and MModality metrics).

We provide the facial motion generation metrics in Table 9. Our facial motions have expressive capabilities and satisfy the textual descriptions. Nonetheless, the quality of generated facial motions and alignment with text could be improved. We leave this as our future work.

	FID	Top1	Top2	Top3	Matching-score	MModality	Diversity
GT	-	0.351 \pm 0.001	0.605 \pm 0.001	0.776 \pm 0.001	1.159 \pm 0.001	-	11.661 \pm 0.091
HumanTOMATO	21.418 \pm 0.038	0.162 \pm 0.001	0.283 \pm 0.001	0.372 \pm 0.001	6.643 \pm 0.003	0.570 \pm 0.025	8.098 \pm 0.085

Table 9: Facial motion generation results on Motion-X dataset.

In the main paper, we compare our method with baseline methods with key-frame sequence visualization. We provide more comparison in Figure 8. In Figure F, the lighter colors represent earlier snapshots. As can be seen, T2M-GPT lacks temporal sensitivity and will generate motions that do not match the text description. In contrast, our method will enjoy these scenarios well and generate vivid motions well aligned with texts.

Additionally, we visualize more generated results of HumanTOMATO in Figure 9 and Figure 10, which show our good generation performance.

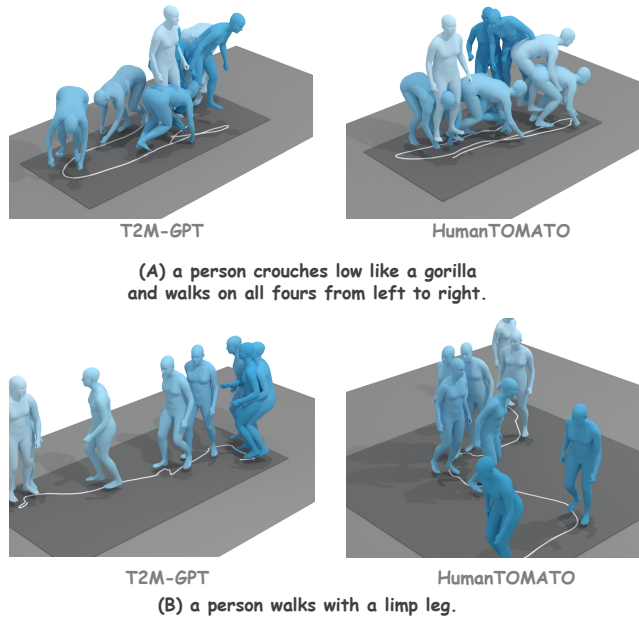


Figure 8: Qualitative comparison with T2M-GPT.

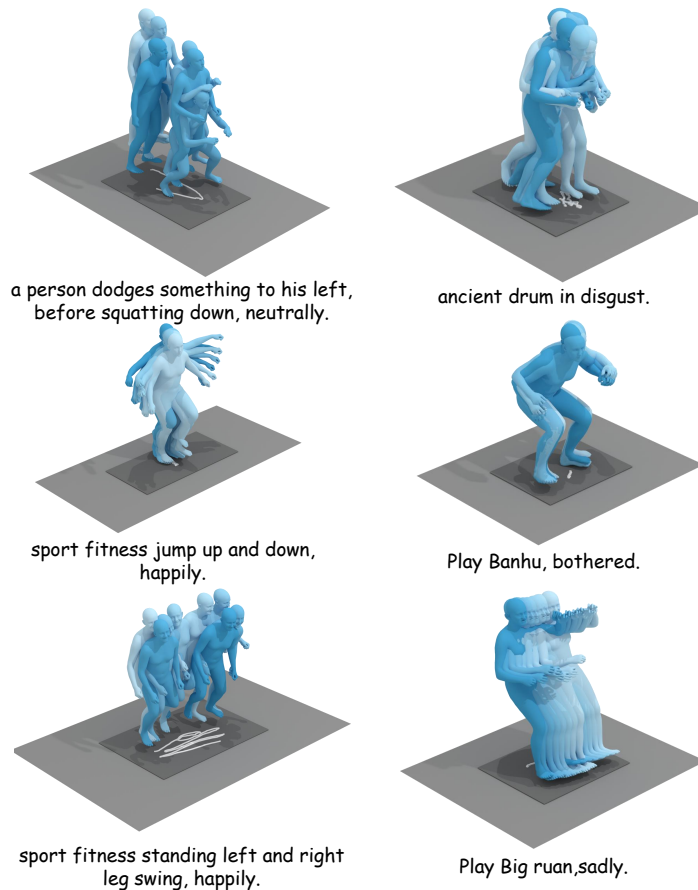


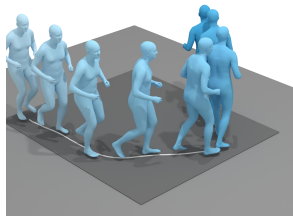
Figure 9: Visualization of the whole-body motions generated by HumanTOMATO (1).



play electric guitar, happily.



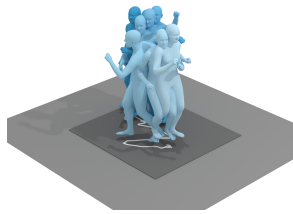
stick figure stood still moving his arms in a strumming motion, unsure.



a person walks slowly in a half circle counterclockwise while holding something, in disgust.



a person looks to be petting a dog with right hand, happily.



a person was dancing on the place while raising the hands up, sadly.



a man grabs an object above his head with his right hand, sadly.

Figure 10: Visualization of the whole-body motions generated by HumanTOMATO (2).

G COMPARISON ON DIFFERENT VECTOR QUANTIZATION METHODS (RQ2)

In the main paper (Section 3.4), we report the MPJPE for evaluating the reconstruction error of Vanilla VQ, RVQ, and H^2VQ respectively. Although HumanML3D only includes body-part motions, we compare the Vanilla VQ-VAE with the RVQ technique to verify our motivation on hierarchical motion modeling, whose results are shown in Table 12. Additionally, as shown in Table 10 and Table 11, we provide more evaluation metrics on PA-MPJPE and Acceleration error (Accel.) (Gower, 1975; Lin et al., 2023a; Zeng et al., 2022; Chen et al., 2023b). to evaluate the reconstruction quality. Evaluation results show that naïvely increasing the codebook size is almost in vain, and hierarchical modeling is effective for action modeling. Besides, our H^2VQ is a better design on whole-body motions than RVQ.

	MPJPE			PA-MPJPE			Accel.		
	All↓	Body ↓	Hand↓	All ↓	Body ↓	Hand ↓	All ↓	Body ↓	Hand↓
Vanilla VQ (512)	140.66	92.20	46.45	58.23	47.72	17.03	23.73	19.99	26.46
Vanilla VQ (1024)	139.33	91.77	46.40	57.30	46.79	17.01	23.54	19.71	26.35
RVQ	110.94	73.97	40.01	40.63	35.84	14.46	21.22	17.76	23.75
H^2VQ	92.97	62.34	37.20	34.21	30.76	14.05	18.95	16.53	20.72

Table 10: Different vector quantization methods on Motion-X.

	MPJPE			PA-MPJPE			Accel.		
	All↓	Body ↓	Hand↓	All ↓	Body ↓	Hand ↓	All ↓	Body ↓	Hand↓
Vanilla VQ (512)	78.23	38.29	31.48	35.32	21.75	14.51	11.01	7.32	13.71
Vanilla VQ (1024)	76.01	37.34	29.89	33.42	20.92	14.14	10.70	7.23	13.25
RVQ	62.94	31.12	27.28	25.61	15.96	13.06	8.80	6.67	10.37
H^2VQ	46.74	24.33	24.59	22.00	13.95	13.48	10.11	6.05	13.09

Table 11: Different vector quantization methods on GRAB.

	MPJPE (Body)↓	PA-MPJPE (Body) ↓	Accel. (Body)↓
Vanilla VQ (512)	77.209	45.53	8.36
Vanilla VQ (1024)	71.34	40.75	7.59
RVQ	63.05	30.99	6.46

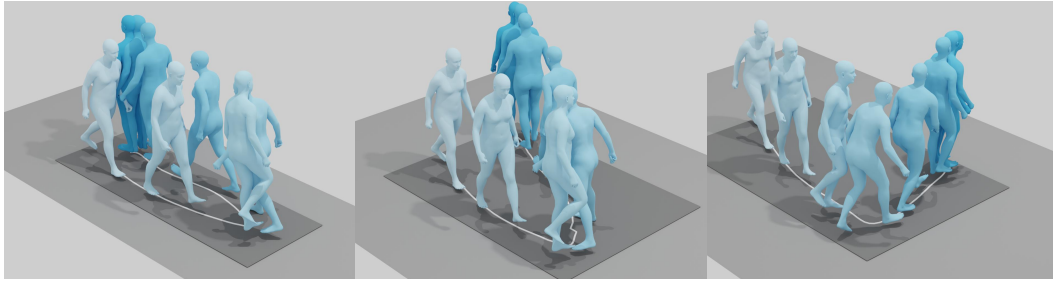
Table 12: Different vector quantization methods on HumanML3D.

We additionally discuss how the H^2VQ helps the motion generation from the aspect of motion quality and text-motion alignment. We take the T2M-GPT as the baseline and compare it to the hierarchical reconstruction setting. The difference between the two settings is with or without the H^2VQ method. As shown in Table 13, the H^2VQ helps both motion generation and text-motion alignment significantly.

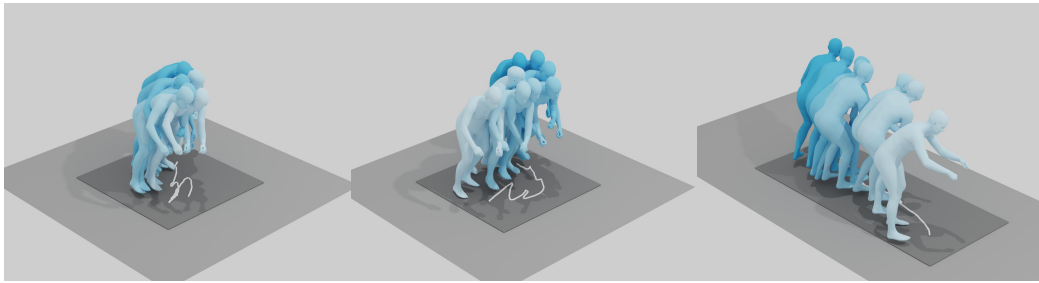
	FID↓	TMR-R-Precision ⁽²⁵⁶⁾			R-Precision ⁽³²⁾			TMR-Matching ↓	Matching ↓
		Top1↑	Top2↑	Top3↑	Top1↑	Top2↑	Top3↑	Score	Score
GT	-	0.500	0.708	0.814	0.407	0.578	0.673	0.768	2.888
T2M-GPT w/o H^2VQ	1.366	0.368	0.553	0.655	0.310	0.446	0.527	0.881	4.316
T2M-GPT w/ H^2VQ	1.086	0.405	0.588	0.695	0.345	0.490	0.573	0.844	3.917

Table 13: The ablation on how can H^2VQ help the whole-body motion generation on T2M-GPT.

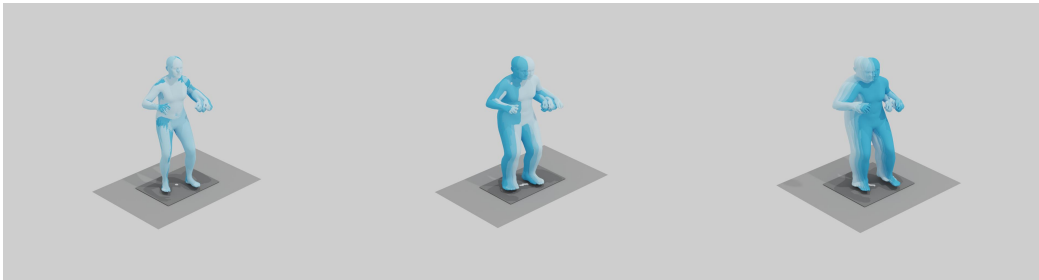
We show more visualization results here. Our method excels in two perspectives, body-part reconstruction and hand-part reconstruction. On the one hand, From 11a, our method H^2VQ in the middle column achieves a significantly higher level of accuracy in reconstructing global translation. From 11b, our method could perform better on movement direction reconstruction and motion coherence. From 11c, our method could reconstruct motion more precisely than other methods even with minor motion movements. On the other hand, because of our decoupled design, our method performs better on hand movement and pose reconstruction. As shown in 12, ours (in blue) can precisely reconstruct the GT hand pose (in green), while the Vanilla VQ-VAE method fails in most of these cases, which demonstrates the superiority of our design.



(a) Case 1. H^2VQ performs better on trajectory reconstruction. (GT, H^2VQ , and Vanilla VQ)



(b) Case 2. H^2VQ performs better on direction reconstruction and motion coherence. (GT, H^2VQ , and Vanilla VQ)



(c) Case 3. H^2VQ performs better on reconstructing motions with low amplitude. (GT, H^2VQ , and Vanilla VQ)

Figure 11: Visualization of motion reconstruction on the Motion-X dataset (body motion reconstruction perspective). From the left to right are GT, H^2VQ , and Vanilla VQ, respectively.

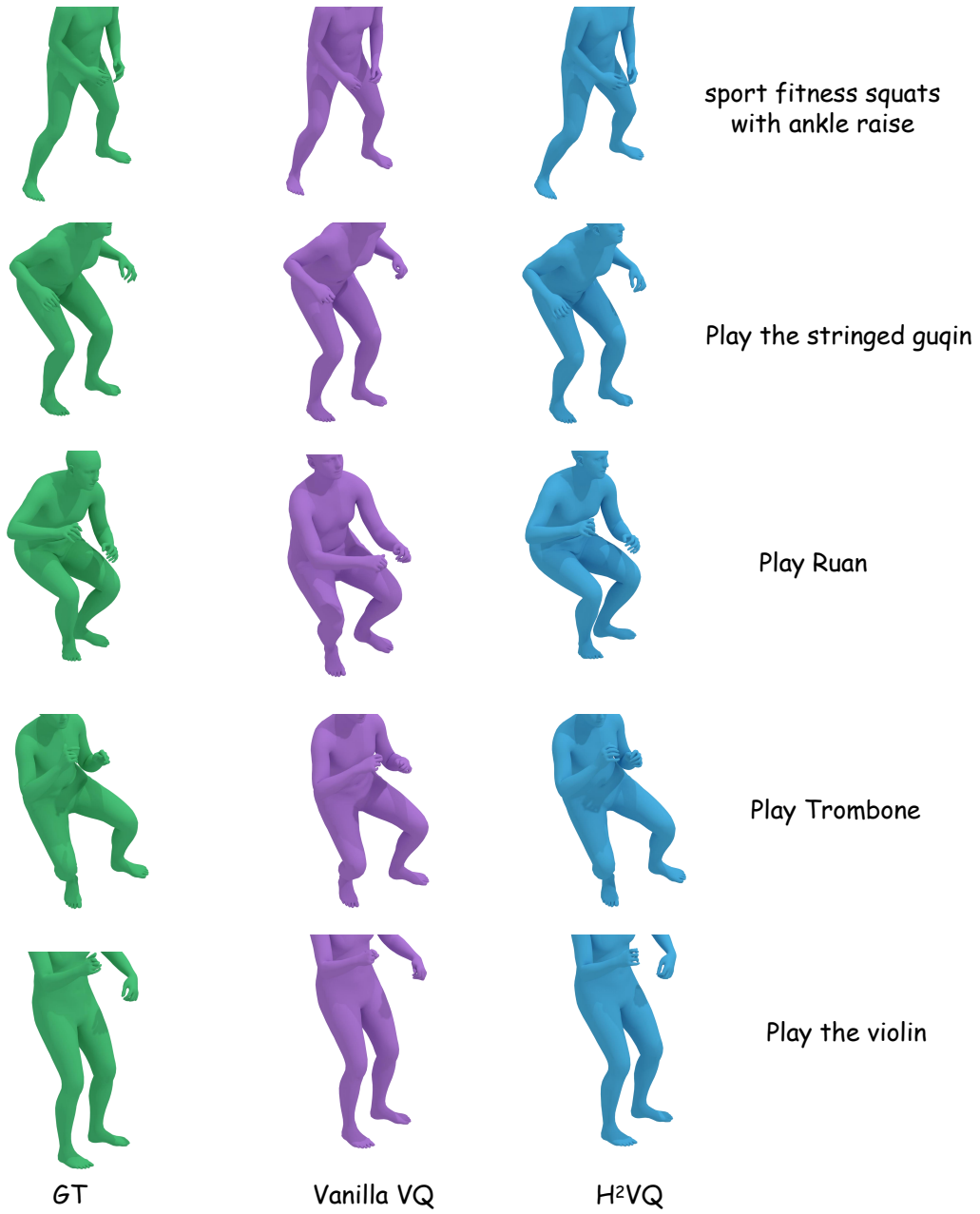


Figure 12: Visualization of motion reconstruction on the Motion-X dataset (hands motion reconstruction perspective). From the left to right are GT, Vanilla VQ, and H²VQ, respectively.

H TEXT-MOTION RETRIEVAL MODEL AS A PRIOR (RQ3)

H.1 QUANTITATIVE RESULTS ON HUMANML3D

In the main paper, we verify that the pre-trained text-motion-aligned model provides a strong prior to text-aligned whole-body motion generation. Additionally, the text-motion-aligned prior not only benefits the whole-body motion generation but also helps the text-motion alignment in body-only motion generation. We take the T2M-GPT as baseline (line 1 in the Table 14), and we ablate whether the TMR language embedding and text-motion-alignment supervision help to generate the text-aligned body-only motions. As shown in Table 14, our experiments on HumanML3D show that both the motion-aware language prior and the text-motion-alignment supervision help to generate higher quality and text-aligned motions (on FID and TMR-R-Precision⁽²⁵⁶⁾).

embedding supervision	FID ↓	TMR-R-Precision ⁽²⁵⁶⁾			R-Precision ⁽²⁵⁶⁾			TMR-Matching-score ↓	Matching-score ↓	
		Top1 ↑	Top2 ↑	Top3 ↑	Top1 ↑	Top2 ↑	Top3 ↑			
CLIP	✗	0.474	0.082	0.129	0.168	0.169	0.259	0.341	1.322	3.155
TMR	✗	0.326	0.147	0.206	0.269	0.177	0.281	0.396	1.285	2.915
TMR	✓	0.312	0.159	0.223	0.276	0.184	0.292	0.396	1.282	2.906

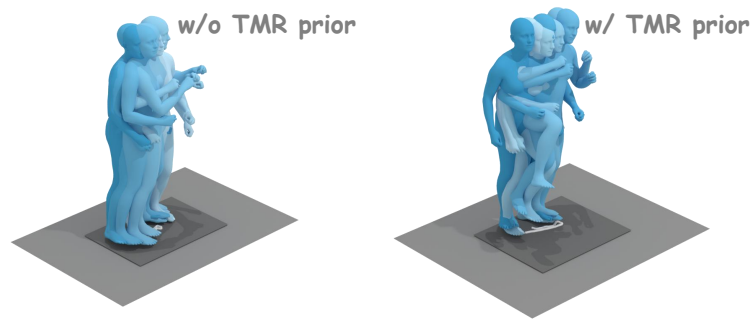
Table 14: Ablation on how pre-trained text-motion aligned model helps to generate the text-aligned body-only motion (on HumanML3D).

H.2 PRE-TRAINED TEXT-MOTION RETRIEVAL MODEL AS A PRIOR

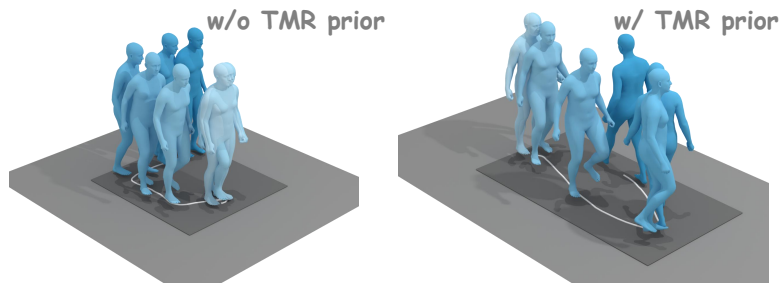
We test on the Motion-X dataset first to explore whether our text-motion-aligned text encoder helps the generated motions align well with the given text. As shown in Figure 13(a), the model with our design performs the “kick” motion. As shown in Figure 13(b) and Figure 13(c), HumanTOMATO learning with motion-aware language prior has a better understanding of motion trajectory and temporal relations.

We test some cases in the wild to explore whether our text-motion-aligned text encoder helps the generated motions align well with the given text. We show some cases for comparison in Figure 14. In Figure 14a, if T2M-GPT learns without motion-aware language prior, the person walks in a quarter of counter-clockwise circle. The model with motion-aware language prior will generate the motion well aligned with the given text on direction and trajectory. For the second case in Figure 14b, our design helps the model to generate motions much better in the motion direction. For the third case, our method is better aligned with text on the caption “back” and does not switch the left or right backward direction.

In summary, as claimed in Section 2.4, our method can understand the motion dynamic clues better on sequentiality, directions, and dynamics.

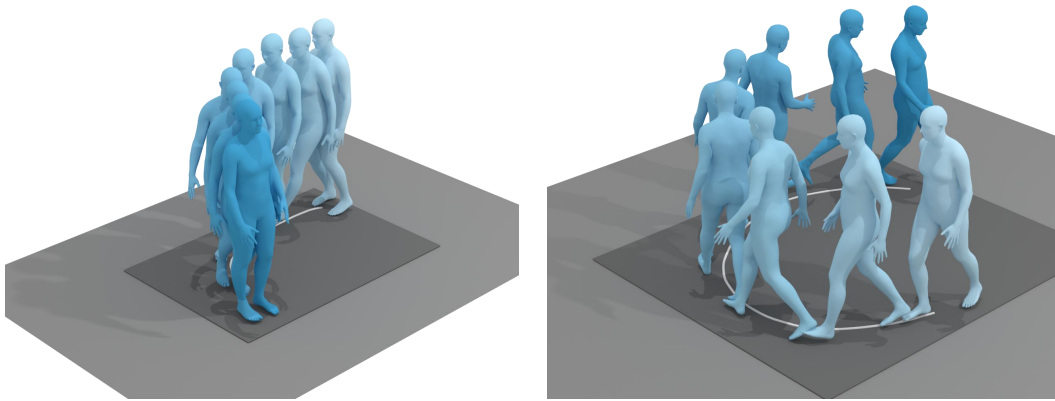


(A) a person performs a standing kick.

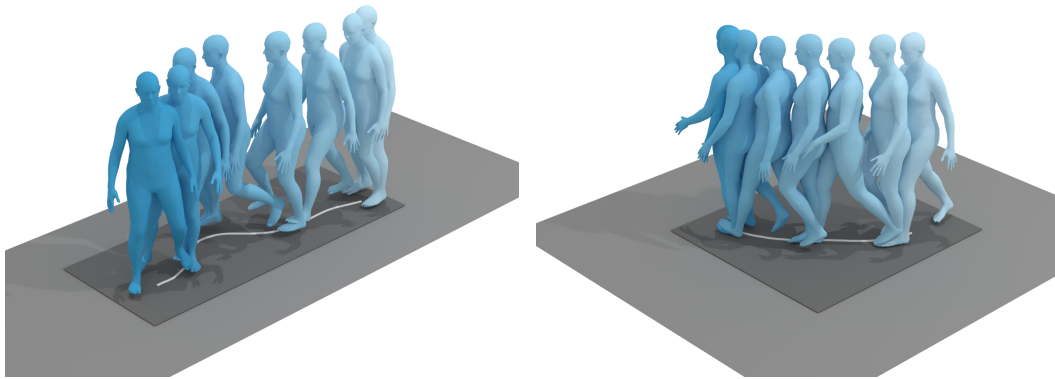


(B) The man walks forward a couple steps, turns right 180 degrees and then walks back.

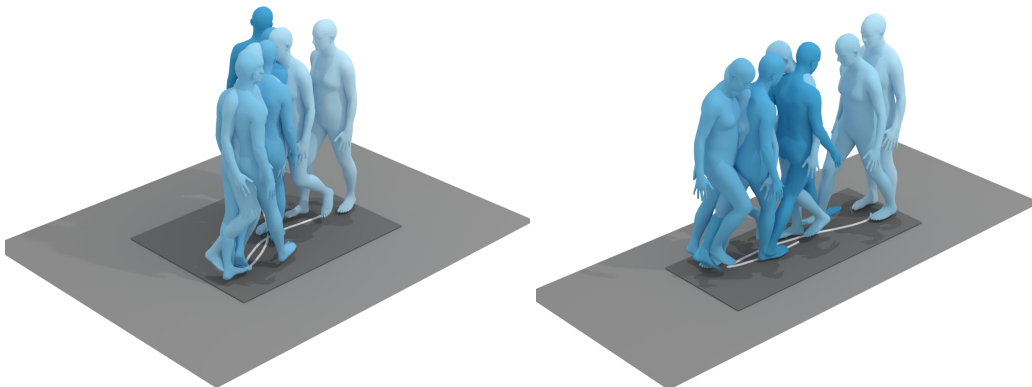
Figure 13: Visualization on our HumanTOMATO, learning without (left) or with (right) motion-aware language prior. The left is the generated motion of HumanTOMATO without language prior, and the right is HumanTOMATO.



(a) Input text: “a person walks clockwise.”. The left is the generated motion of T2M-GPT, and the right is T2M-GPT learning with motion-aware language prior.



(b) Input text: “a person walks forward, turn right, finally turn right.”. The left is the generated motion of T2M-GPT, and the right is T2M-GPT learning with motion-aware language prior.



(c) Input text: “A person walks forward and then turns back.”. The left is the generated motion of T2M-GPT, and the right is T2M-GPT learning with language prior.

Figure 14: Visualization on T2M-GPT, learning without (left) or with (right) motion-aware language prior. The left is the generated motion of T2M-GPT, and the right is T2M-GPT learning with language prior.

I DETAILS ON THE EVALUATION METRICS (RQ4)

In Section 3.6, we analyze why the proposed evaluation metrics of alignment between generated motions and given texts are more accurate and challenging on the Motion-X dataset. Here, we provide more comparisons on both body-only and whole-body datasets to verify the universality of the proposed metrics, all of which are calculated 3 times to calculate the mean and standard value ($mean^{\pm std}$). The comparison is shown in Table 15 and Table 16. We also visualize the comparison on the HumanML3D dataset in Figure 15. Similar to the conclusion in Section 3.6, our metrics are more accurate and challenging than Guo et al. (2022)’s in the following two aspects. (1) $TMR-R-Precision^{(B)}$ and $TMR-Matching-score^{(B)}$ metrics are more accurate than Guo et al. (2022)’s $R-Precision^{(B)}$ and $Matching-score$ metrics. (2) $B = 256$ is a more challenging retrieval setting than the $B = 32$ setting.

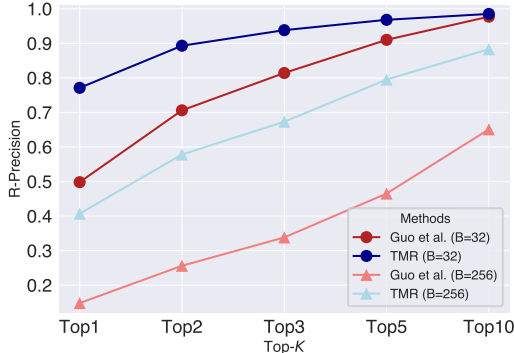


Figure 15: Comparison with existing metrics on HumanML3D. Existing evaluation metrics (Guo et al., 2022) are illustrated in red and ours are in blue. The $B = 32$ and $B = 256$ settings for retrieval are denoted as “●” and “▲” respectively.

	Top1	Top2	Top3	Top5	Top10
Guo et al. (2022) $B = 32$	0.498 \pm .006	0.706 \pm .005	0.814 \pm .003	0.910 \pm .003	0.977 \pm .001
TMR $B = 32$	0.771\pm.001	0.893\pm.003	0.938\pm.002	0.968\pm.001	0.985\pm.000
Guo et al. (2022) $B = 32$	0.148 \pm .002	0.256 \pm .004	0.338 \pm .004	0.465 \pm .003	0.651 \pm .002
TMR $B = 256$	0.407\pm.003	0.578\pm.004	0.673\pm.003	0.795\pm.001	0.883\pm.001

Table 15: R-Precision of GT motions and texts on the Motion-X dataset.

	Top1	Top2	Top3	Top5	Top10
Guo et al. (2022) $B = 32$	0.511 \pm .003	0.705 \pm .002	0.795 \pm .003	0.887 \pm .003	0.964 \pm .003
TMR $B = 32$	0.711\pm.005	0.853\pm.001	0.905\pm.002	0.947\pm.001	0.977\pm.001
Guo et al. (2022) $B = 256$	0.167 \pm .002	0.279 \pm .002	0.368 \pm .003	0.490 \pm .004	0.659 \pm .003
TMR $B = 256$	0.365\pm.003	0.527\pm.002	0.625\pm.004	0.731\pm.003	0.838\pm.002

Table 16: R-Precision of GT motions and texts on the HumanML3D dataset.

J BROADER IMPACT AND LIMITATION

In this section, we will discuss the border impact and limitations.

Broader Impact. On the one hand, we explore the whole-body motion generation task and leverage the large-scale whole-body mocap dataset Motion-X to pre-train a motion-text-aligned prior. These could be a foundation for the field-related research community. Besides, based on the motion reconstruction via the proposed discrete latent compression scheme of human motions and large-scale motion data training, the pre-trained HumanTOMATO can provide motion prior, like VPoser (Pavlakos et al., 2019). It can also benefit Motion Capture models (Lin et al., 2023b; Yang et al., 2023) denoising and reducing the impact of noisy annotation (Xia et al., 2020; 2019; Li et al., 2022). On the other hand, expressive, text-controllable, and high-quality motion generation can be implemented for many practical application scenarios, such as motion generation for games and animations, robotics, and motion interaction.

Limitation. Although this work makes great progress on the novel task, and the significant improvement of motion reconstruction and text-aligned generation, it still has some shortcomings. First, the natural textual description utilization for whole-body motion generation needs to be further explored. This work simply uses the sequential semantic descriptions following previous works without frame-level or fine-grained whole-body descriptions. Second, the face generation lacks a unified generation scheme. Due to the limited holistic facial expression data and face motion descriptions (e.g., only commonly used emotion here), a simple condition VAE is not the best design choice. As rich data comes, a unified framework could be future work. Additionally, we will unify more text-motion-pairwise data⁵ for training a better motion generation model.

⁵<https://github.com/LinghaoChan/UniMoCap>.